國立臺灣大學工程學院化學工程學系

碩士論文

Department of Chemical Engineering

College of Engineering

National Taiwan University

Master Thesis

批次結晶程序整體設計之發展

Development of recipes for seeded batch crystallization

曾郁迪

Yu-Ti Tseng

指導教授：吳哲夫 博士

Advisor: Jeffrey D. Ward, Ph.D.

中華民國 100 年 7 月

July, 2011

誌謝

非常感謝吾師 吳哲夫教授，在這兩年時間給我很多指導，讓我在研究方面能有自由發揮的空間，做人處事方面也是我的學習標的。另外感謝陳誠亮教授、錢義隆教授與黃孝平教授帶給我們的研究環境。

在此我非常感謝家人對我的支持，你們的鼓勵，是我堅持下去的動力，接者感謝同窗: 傳真祝你當兵順利；宗翰煙少抽一點吧：哲維教我彈吉他吧；香腸我會懷念你超好笑的嘴砲；達叔不愧是俄羅斯方塊之神；育賢我會懷念你生氣的樣子超搞笑；鎮宇，喔醬、這樣尼。

最後感謝學長姊們（ 豪業、建凱、乾元、義章、士暐、瑞元、志曜、愷悌、玉龍、雅玲、Anton、佳紘、國超、昱峰、明璟、媛翎、詩雯、Anggi ）與學弟們（ 恒嘉、紹群、偉倫、子軒、桐霖、旻澤、滕允 ）。很高興能加入溫馨的 PSE 實驗室，能夠認識你們大家是一生的福氣。

摘要

在此研究中我們對於批次結晶程序做了整體性的分析及探討。首先我們探討了給予長晶速率限制條件對程序的影響。對於特定操作條件我們發現增加限制條件對於產品品質沒有顯著影響。接著我們探討晶種負載率的影響。我們發現提高晶種負載率能更有效率壓制成核以及成核速率。另外此研究中我們透過電腦模擬針對兩個結晶系統以及無因次系統做了晶種分析圖。對於臨界晶種負載率我們導出無因次的關係式，研究發現此關係式對於預測模擬結果有很高的準確度。我們探討了臨界晶種總表面積以及臨界晶種總長度，然而這兩個變數不建議做為設計變數。此研究中我們也探討了總反應時間以及淨結晶產量對於批次結晶程序的影響，結果可用做設計結晶程序的簡單方針。

關鍵字：長晶速率限制;臨界晶種負載率;總反應時間;淨結晶產量。

Abstract

In this work we investigate the development of recipes for seeded batch crystallization processes. First we investigate the effect of growth rate constraint. For a particular case we find that such a constraint does not have a significant influence on product quality. Then we investigate the effect of seed loading. We find that the seed mass has a large influence on decreasing the final nuclei mass and efficiently suppressed the nucleation rate. In this work seed charts for two dimensional systems and the dimensionless system are produced and used to determine critical seed loading ratio by computer simulation. An analytical expression for the critical seed loading is derived and simulation results show high accuracy for predicting critical seed loading ratio versus dimensionless seed mean size using constant growth rate trajectory. We investigate two critical values which are critical seed surface area and critical seed total length. However these two critical values are not recommended to use as the design variables. In this work we also investigate the effect of total batch time and the net crystal yield on the batch process, and the results can be used as the design guideline.

Keywords: growth rate constraint, critical seed loading ratio, total batch time, the net crystal yield.

Table of Content

List of Figures

List of Tables

1 Introduction

1.1 Overview

Crystallization is an important unit operation in industry, due to its ability to provide high purity separations. While large-scale processes operate with continuous crystallizers, the majority of crystallization processes are operated in batch-wise. Batch crystallization processes are usually operated with seed charged at the beginning to improve the performance, so the process is called seeded batch crystallization. The driving force of crystallization is the supersaturation of the solution. This driving force drives the growth of crystals and also causes the formation of new small crystals called nuclei. This process is called nucleation. Supersaturation can be induced by cooling, solvent evaporation, introduction of anti-solvent or by other methods. In crystallization processes, crystal size distribution (CSD) is a critically important factor to measure the quality of products, and also affects the efficiency of downstream process.

In batch cooling crystallization an important consideration is how the supersaturation (or temperature) should change with time. There are several ways to determine the trajectory of temperature versus batch time for the whole process. The following Figure shows different temperature trajectories, which are linear cooling,

controlled cooling and natural cooling. Here the controlled cooling is defined as

$$T(t) = T(0) + (T(t_f) - T(0))\left(\frac{t}{t_f}\right)^3 \qquad (1\text{-}1)$$

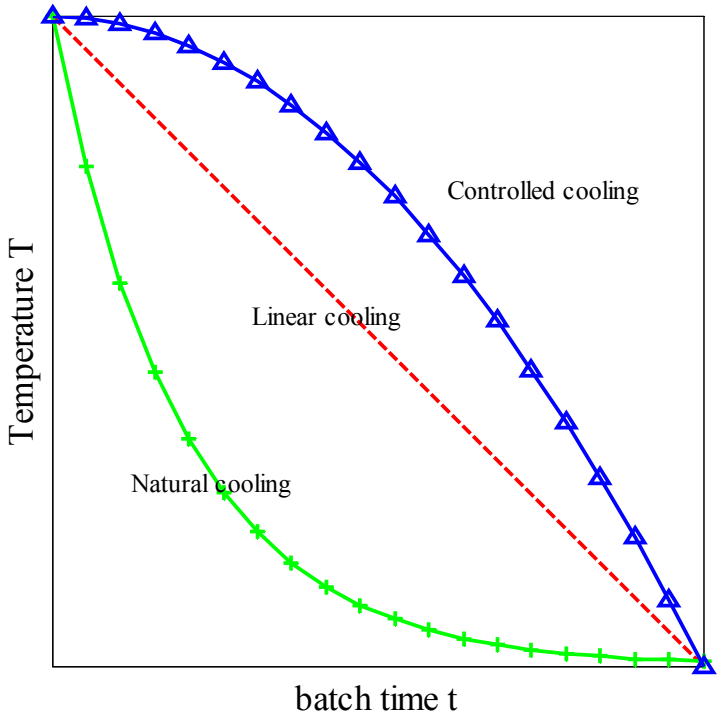

Figure 1-1 Cooling curve for different temperature trajectories

In our research we use linear cooling of temperature or linear concentration to the corresponding temperature trajectory as the temperature trajectories since in many published papers researchers conducted the experiments by using uncontrolled cooling (natural cooling) as the temperature trajectory, and the fact that natural cooling performs worse than linear cooling. There is a limitation in operating batch crystallization process: the concentration of the crystal is not allowed to exceed the metasTable limit because it would cause the spontaneous nucleation (primary

nucleation), which is undesired.

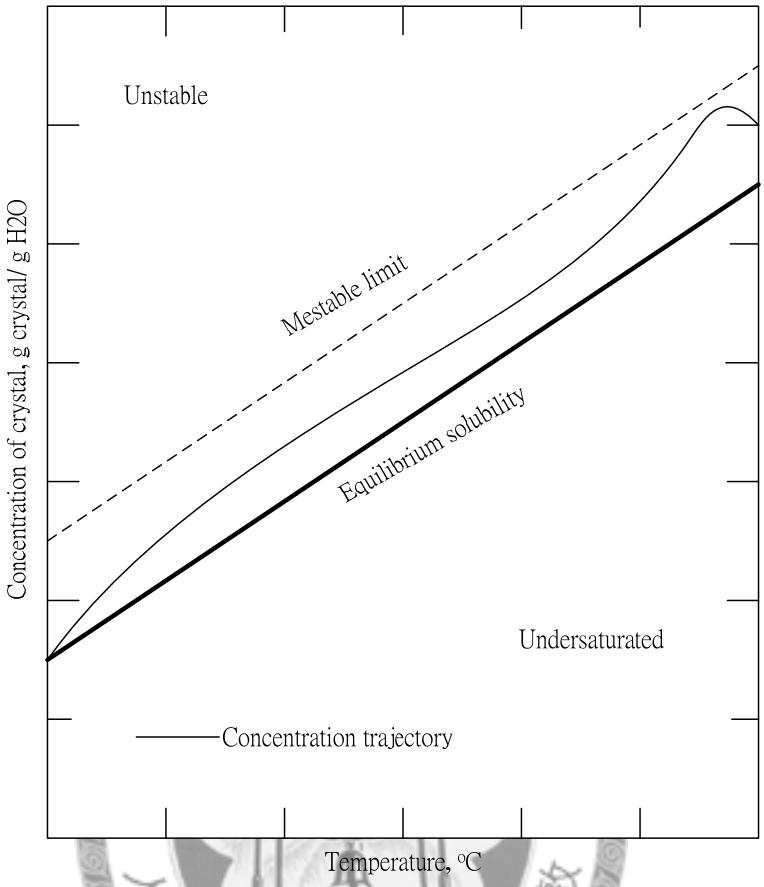

Figure 1-2 Solubility-supersolubility diagram for batch cooling crystallization

There is another important issue in operating the seeded batch crystallization, which is the effect of the seed properties on the whole process. Several authors published results in which they stated that optimizing seed properties can improve the performance and may be more important than optimizing the supersaturation trajectory. In this study, we focus research on the effect of seed properties.

1.2 Seeding policy

The seed distribution used in this study is the parabolic distribution since its

simplicity to implement. There are three parameters of seed properties generally used for describing parabolic distribution: seed number mean size, seed mass and seed width. Seeding policy is to generally give seeding conditions to guarantee a good result of batch crystallization process.

Determine seeding condition such as seed mean size or seed mass of batch crystallization process is called seeding policy. Seeding policy is getting more attention until recent years compared to the cooling policy. In last decade research papers dealing with the seeding effects were few, and those were published by Jagadesh et al. [1, 2], Kubota and coworkers et al. [3-10], Lung-Somarriba et al. [11], Hojjati and Rohani [12], Chung et al. [13] and so on. The most important result of these papers is that if the seed loading is greater than a specific value called “critical seed loading”, then secondary nucleation in the process is efficiently suppressed, i.e., seed crystals grow essentially without generation of nuclei (fine particles). Another important issue is that the product crystal size distribution (CSD) is strongly influenced by the seed. Kubota and coworkers proposed an equation which describes the ideal-growth line and is derived analytically, and seed charts were plotted using experimental data. In this study, we reproduce the seed charts of different crystal systems by simulation, and also determine the empirical Equation.

1.3 Literature survey

Mullin and Nyvlt [14] in 1971 proposed a programmed cooling by a simple mathematical description to improve the performance of batch crystallization processes, and they also conducted a experiment which demonstrated the potential of using programmed cooling to give a large improvement compared to uncontrolled cooling.

Chung et al. were the first researches to use seed parameters as variables for optimization of a batch crystallization process, and they concluded that optimizing the seed properties has a larger effect on product CSD than optimizing the supersaturation profile. They also analyzed how seed properties such as mean size of seed crystals, seed mass, and the width of the seed distribution affect product CSD.

Kubota and coworkers published several papers about producing seed charts and the effect of seed loading ratio C_s, which is the seed mass divided by crystal yield. The definition of crystal yield is the theoretical amount we can get from a single batch process. They found that if the seed loading ratio C_s is greater than a critical value C_s*, unimodal grown seeds can be obtained, and the impact of the cooling mode (temperature trajectory) becomes relatively small. Kubota and Doki in 2001 stated that different cooling modes have no influence if the seed loading is high enough.

Another important issue Kubota and Doki concluded is that from the seed chart for a particular crystal system, one can easily determine an empirical Equation which describes the relationship between critical seed loading ratio C_s^* and seed volume mean size L_s. This Equation can be used to design the batch process without other information such as kinetic parameters.

Hojjati and Rohani in 2005 had similar results as Kubota and coworkers. They concluded that increasing the seed loading would decrease the peak of supersaturation, reduce the nucleation rate and increase the growth rate for all different cooling modes (temperature trajectories). The difference is that they concluded that although cooling modes have no influence on the process when the seed loading ratio is higher than the critical ratio, using a controlled cooling policy rather than linear or natural cooling can produce a larger product mean size and decrease C_s^* observed from experimental results.

Lung-Somarriba et al. proposed a different variable to be controlled rather than critical seed loading ratio. They proposed a specific value called critical seed surface area S_c which suppresses nucleation if the seed surface area exceeds S_c. But there is a limitation: the seed size must be small enough to achieve a good result even though the seed surface area reaches S_c.

Ward et al [15] proposed a generalized dimensionless model of a seeded batch crystallization process to analyze the crystallization systems independent of system parameters. Here we summarize two concluding remarks from the study: The Mullin-Nyvlt trajectory can be implemented without kinetic data and gives a good result if seed properties are also favorable. Another point is optimizing seed properties is more important than the supersaturation trajectory.

1.4 Thesis Organization

In this thesis the subjects can be separated into six main parts: First part is to investigating the effect of growth rate constraint. Second part is to do some case study systems. Third part is to reproduce seed chart and then determine empirical Equation for both real crystal systems and dimensionless system. Fourth part is the analytical expressions of critical seed loading ratio. Fifth part is the discussion of critical surface area. Sixth part is to combine all the information and conclusions from several research papers to analyze the effect of seed properties on the batch crystallization process and then give a general guideline to design or predict the seeded batch crystallization process.

2 Modeling of crystallization systems

This section presents a brief summary of the model generally used for modeling the batch crystallization. The method of moments is originally from Hulbert and Katz [16]. Other background information needed is in reference texts [17-21].

In the absence of agglomeration and breakage of crystals, a general expression for population balance for a well-mixed batch crystallization system is:

$$\frac{\partial f(L,t)}{\partial t} + \frac{\partial (G(L,t) f(L,t)}{\partial L} = 0 \qquad (2\text{-}1)$$

Where f (L,t) is the crystal size distribution (CSD) function and G is crystal growth rate (m/s). Equation 2-1 is subject to an initial condition based on the properties of seeds at the beginning of the batch, and to a left boundary condition:

$$f(0,t) = \frac{B(f(L,t),t)}{G(0,t)} \qquad (2\text{-}2)$$

B is nucleation rate (#/m^{3}s). Definition of supersaturation, which is the driving force for both nucleation rate and crystal growth is:

$$S = C - C_{sat} \qquad (2\text{-}3)$$

And common expressions for crystal growth rate and secondary nucleation are:

$$G = k_g S^g \tag{2-4}$$

$$B = k_b G^\gamma \mu_3 \tag{2-5}$$

where k_g, g, k_b, and γ are empirically determined kinetic parameters, and μ_3 is the third moment of crystal size distribution. The definition of the moment is:

$$\mu_i = \int_0^\infty L^i f(L) dL \quad i = 0,1,2... \tag{2-6}$$

and expressions for the time evolution of the moments (if crystal growth is independent of crystal size) are:

$$\frac{d\mu_0}{dt} = B \tag{2-7}$$

$$\frac{d\mu_i}{dt} = iG\mu_{i-1} \quad i = 1,2,... \tag{2-8}$$

An expression for a mass balance on the solute is

$$\frac{dC}{dt} = -3\rho_c k_v \mu_2 \tag{2-9}$$

For the seed-grown crystals (subscript s) and nuclei-grown crystals (subscript s), the expressions are:

$$\frac{d\mu_{s,0}}{dt} = 0 \tag{2-10}$$

$$\frac{d\mu_{s,i}}{dt} = iG\mu_{s,i-1} \quad i = 1,2,... \tag{2-11}$$

$$\frac{d\mu_{n,0}}{dt} = B \tag{2-12}$$

$$\frac{d\mu_{n,i}}{dt} = iG\mu_{n,i-1} \quad i = 1,2,... \tag{2-13}$$

Note that for each moment, the total crystal value equals the seed-grown value

plus nuclei-grown value:

$$\mu_{T,i} = \mu_{n,i} + \mu_{S,i} \tag{2-14}$$

In this work, in order to generalize the analysis, we use the dimensionless model derived by Ward et al. (2011) in our simulation. Start by defining all concentrations relative to the concentration at the end of the batch like following

$$C^{\dagger} = C - C_f \tag{2-15}$$

$$C' = \frac{C - C_f}{C_0 - C_f} \tag{2-16}$$

So the dimensionless concentration decreases from 1 to 0 during the process. Then define dimensionless time,

$$t' = t/t_f \tag{2-17}$$

And a reference variable for the third moment

$$\bar{\mu}_3 = \frac{C_0^{\dagger}}{\rho_c k_v} = \frac{\left(C_0 - C_f\right)}{\rho_c k_v} \tag{2-18}$$

so the dimensionless third moment is expressed as

$$\mu_3' = \frac{\mu_3}{\bar{\mu}_3} \tag{2-19}$$

The reference variable for growth rate and dimensionless growth rate are

$$\bar{G} = \left(k_b t_f^4\right)^{\frac{-1}{\gamma+3}} \tag{2-20}$$

$$G' = \frac{G}{\bar{G}} \tag{2-21}$$

Then define reference variable for nucleation rate

$$\bar{B} = k_b \bar{\mu}_3 \left(k_b t_f^4\right)^{\frac{-\gamma}{\gamma+3}} \tag{2-22}$$

$$B' = \frac{B}{\bar{B}} = \frac{B}{k_b \bar{\mu}_3 \left(k_b t_f^4\right)^{\frac{-\gamma}{\gamma+3}}} \tag{2-23}$$

We further define reference variables for the moments:

$$\bar{\mu}_0 = \bar{B} t_f \tag{2-24}$$

$$\bar{\mu}_1 = \bar{B}\bar{G} t_f^2 \tag{2-25}$$

$$\bar{\mu}_2 = \bar{B}\bar{G}^2 t_f^3 \tag{2-26}$$

$$\bar{\mu}_3 = \bar{B}\bar{G}^3 t_f^4 \tag{2-27}$$

Here we check the consistency of the definitions by substituting Equation 2-20 and 2-22 into Equation 2-27:

$$\bar{B}\bar{G}^3 t_f^4 = k_b \bar{\mu}_3 \left(k_b t_f^4\right)^{\frac{-\gamma}{\gamma+3}} \left(k_b t_f^4\right)^{\frac{-3}{\gamma+3}} t_f^4 = \bar{\mu}_3 \tag{2-28}$$

With these definitions, the differential Equations for the time evolution of the moments of the crystal size distribution become:

$$\frac{d\mu_0'}{dt'} = B' = (G')^{\gamma}\ \mu_3' \tag{2-29}$$

$$\frac{d\mu_1'}{dt'} = G'\mu_0' \tag{2-30}$$

$$\frac{d\mu_2'}{dt'} = 2G'\mu_1' \tag{2-31}$$

$$\frac{d\mu_3'}{dt'} = 3G'\mu_2' \tag{2-32}$$

The same derivation can also be applied to $\mu_{s,i}$ and $\mu_{n,i}$ respectively. The following Table shows definitions of all reference variables and dimensionless variables.

Table 2-1 Definitions of reference variables and dimensionless variables

reference variables	dimensionless variables	
$\bar{G} = \left(k_b t_f^4\right)^{\frac{-1}{\gamma+3}}$	$t' = t/t_f$	$m_s' = m_s/\left(C_0 - C_f\right)$
$\bar{\mu}_3 = \left(C_0 - C_f\right)/\left(\rho_c k_v\right)$	$B' = B/\bar{B}$	$x_0' = x_0/\left(\bar{G}t_f\right)$
$\bar{B} = k_b\bar{\mu}_3\left(k_b t_f^4\right)^{\frac{-\gamma}{\gamma+3}}$	$G' = G/\bar{G}$	$L' = L/\left(\bar{G}t_f\right)$
$\bar{\mu}_i = \bar{B}\bar{G}^i t_f^{i+1} \quad i = 0,1,2$	$C' = \left(C - C_f\right)/\left(C_0 - C_f\right)$	$f' = \bar{G}f/\bar{B}$
	$\mu_i' = \mu_i/\bar{\mu}_i$	$w' = w/\left(\bar{G}t_f\right)$

In our simulation, the seed crystal size distribution is parabolic as shown in Figure 2-1.

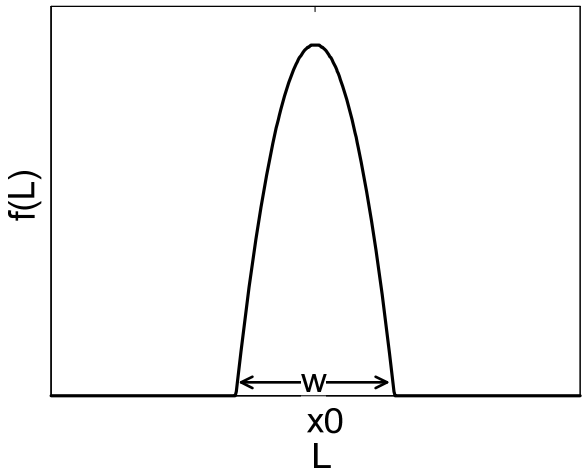

Figure 2-1 Seed crystal size distribution.

We consider the case where the initial seed crystal size distribution function $f(L)$ is parabolic with a width at the base equal to $w < 2x_0$, as shown in Figure 2-1. We also desire that the total mass of the seeds will be equal to m_s. Then the function $f(L)$ is given by:

$$f_0(L) = \begin{cases} 0 & L < x_0 - w/2 \\ -a\left(L - \left(x_0 - \frac{w}{2}\right)\right)\left(L - \left(x_0 + \frac{w}{2}\right)\right) & x_0 - w/2 \le L \le x_0 + w/2 \\ 0 & L > x_0 + w/2 \end{cases} \quad (2\text{-}33)$$

Where a can be determined from the following relation:

$$\int_0^{\infty} L^3 f_0(L) = \int_{x_0 - w/2}^{x_0 + w/2} L^3 f_0(L) = \frac{m_s}{\rho k_v} \quad (2\text{-}34)$$

Solving for *a* gives:

$$a = \frac{m_s}{\rho_c k_v}\left(\frac{1}{6}x_0^3 w^3 + \frac{1}{40}x_0 w^5\right)^{-1} \quad (2\text{-}35)$$

And substituting Equation 2-35 into Equation 2-33 gives:

$$f_0(L) = -\frac{m_s}{\rho_c k_v}\left(\frac{1}{6}x_0^3 w^3 + \frac{1}{40}x_0 w^5\right)^{-1}\left(L-\left(x_0-\frac{w}{2}\right)\right)\left(L-\left(x_0+\frac{w}{2}\right)\right) \quad (2\text{-}36)$$

for $x_0 - w/2 \le L \le x_0 + w/2$. Define:

$$w' = \frac{w}{\bar{G}t_f} \quad (2\text{-}37)$$

Then further define:

$$f'(L,t) = \frac{\bar{G}f(L,t)}{\bar{B}} \quad (2\text{-}38)$$

Substituting the definitions of the dimensionless variables into Equation 2-36 gives:

$$f_0'(L') = -m_s'\left(\frac{1}{6}x_0'^3 w'^3 + \frac{1}{40}x_0' w'^5\right)^{-1}\left(L'-\left(x_0'-\frac{w'}{2}\right)\right)\left(L'-\left(x_0'+\frac{w'}{2}\right)\right) \quad (2\text{-}39)$$

The dimensionless moments of the initial seed crystal size distribution are:

$$\mu_{s,0}'(0) = \frac{20m_s'}{x_0'\left(20x_0'^2 + 3w'^2\right)} \quad (2\text{-}40)$$

$$\mu_{s,1}'(0) = \frac{20m_s'}{\left(20x_0'^2 + 3w'^2\right)} \quad (2\text{-}41)$$

$$\mu_{s,2}'(0) = \frac{m_s'x_0'\left(20x_0'^2 + w'^2\right)}{\left(20x_0'^2 + 3w'^2\right)} \quad (2\text{-}42)$$

$$\mu_{s,3}'(0) = m_s' \quad (2\text{-}43)$$

It is known that nucleation is not only related to the supersaturation, but also the crystals in the batch crystallizer. Ward et al. only consider the situation where the power on the third moment in Equation 2-5 is equal to one. In this section, we discuss the situation that the different magnitude of effect for the nucleation due to the crystal

in the batch crystallizer by adding a variable jj to the Equation 2-5. The Equation will be like this:

$$B = k_b G^{ii} \mu_3^{jj} \tag{2-44}$$

Since the form of B changes, the units of k_b also change.

$$k_b[=]\frac{\#}{m^3 s}\left(\frac{m}{s}\right)^{-ii}\left(\frac{m^3 crystals}{m^3 solution}\right)^{-jj} \tag{2-45}$$

The dimensionless third moment remains the same:

$$\overline{\mu}_3 = \frac{C_0^{\dagger}}{\rho_c k_v} = \frac{\left(C_0 - C_f\right)}{\rho_c k_v} \tag{2-46}$$

Recall the definitions

$$\overline{\mu}_0 = \overline{B} t_f \tag{2-47}$$

$$\overline{\mu}_1 = \overline{B}\overline{G} t_f^2 \tag{2-48}$$

$$\overline{\mu}_2 = \overline{B}\overline{G}^2 t_f^3 \tag{2-49}$$

$$\overline{\mu}_3 = \overline{B}\overline{G}^3 t_f^4 \tag{2-50}$$

We want the dimensionless moment ODE set to be like this:

$$\frac{d\mu_0'}{dt} = B' = \left(G'\right)^{jj} \mu_3' \tag{2-51}$$

$$\frac{d\mu_1'}{dt} = G'\mu_0' \tag{2-52}$$

$$\frac{d\mu_2'}{dt} = 2G'\mu_1' \tag{2-53}$$

$$\frac{d\mu_3'}{dt} = 3G'\mu_2' \tag{2-54}$$

Therefore, we define

$$\overline{G} = \left(k_b \overline{\mu_3}^{jj-1} t_f^4 \right)^{\frac{-1}{ii+3}} \tag{2-55}$$

$$\overline{B} = k_b \overline{\mu}_3^{jj} \left(k_b t_f^4 \right)^{\frac{-ii}{ii+3}} \tag{2-56}$$

The dimensionless crystal birth and crystal growth becomes

$$B' = \frac{B}{\overline{B}} = \frac{B}{k_b \overline{\mu}_3^{jj} \left(k_b t_f^4 \right)^{\frac{-ii}{ii+3}}} \tag{2-57}$$

$$G' = \frac{G}{\overline{G}} = \frac{G}{\left(k_b \overline{\mu_3}^{jj-1} t_f^4 \right)^{\frac{-1}{ii+3}}} \tag{2-58}$$

Note that

$$\overline{B}\overline{G}^3 t_f^4 = k_b \overline{\mu}_3^{j} \left(k_b \overline{\mu}_3^{j-1} t_f^4 \right)^{\frac{-i}{i+3}} \left(k_b \overline{\mu}_3^{j-1} t_f^4 \right)^{\frac{-3}{i+3}} t_f^4 = \overline{\mu}_3 \tag{2-59}$$

Define

$$f'(L) = \frac{\overline{G} f(L)}{\overline{B}} \tag{2-60}$$

The dimensionless initial seed crystal size distribution becomes:

$$f'(L) = -\frac{\overline{G} m_s}{\overline{B}\left(\overline{G} t_f\right)^4 \rho k_v} \left(\frac{1}{6} x_0'^3 w'^3 + \frac{1}{40} x_0' w'^5 \right)^{-1} \left(L' - \left(x_0' - \frac{w'}{2} \right) \right) \left(L' - \left(x_0' + \frac{w'}{2} \right) \right) \tag{2-61}$$

Apply Equation 2-56 and Equation 2-55 we have:

$$f'(L) = -\frac{m_s}{\overline{\mu}_3 \rho k_v} \left(\frac{1}{6} x_0'^3 w'^3 + \frac{1}{40} x_0' w'^5 \right)^{-1} \left(L' - \left(x_0' - \frac{w'}{2} \right) \right) \left(L' - \left(x_0' + \frac{w'}{2} \right) \right) \tag{2-62}$$

with Equation 2-46, the Equation becomes:

$$f'(L) = -m_s' \left(\frac{1}{6} x_0'^3 w'^3 + \frac{1}{40} x_0' w'^5 \right)^{-1} \left(L' - \left(x_0' - \frac{w'}{2} \right) \right) \left(L' - \left(x_0' + \frac{w'}{2} \right) \right) \tag{2-63}$$

Where the parameter of seed distribution function are defined as:

$$m_s' = \frac{m_s}{C_0^\dagger} \tag{2-64}$$

$$x_0' = \frac{x_0}{\bar{G}t_f} \tag{2-65}$$

$$w' = \frac{w}{\bar{G}t_f} \tag{2-66}$$

3 Case study systems

3.1 Case Study

Before discussing the meaning of seed charts, in this section we investigate the effect of seed loading ratio for the region $C_s<C_s^*$. Here we use two groups of parameters for potassium nitrate-water system (Chung et al) and potassium sulphate-water system (Sarkar et al) given in Table 5-1 and Table 5-2.

The following figure shows the comparison of different seed loading, which are 1kg 5kg 10kg seed crystals respectively using Chung's kinetic parameters. Here the temperature trajectory $T(t)$ is linear cooling of temperature, and the seed number mean size L_0 is set to 100μm and the seed CSD is parabolic distribution with width W equal to 20μm. As the seed loading is increased, the peak of supersaturation is lower due to the larger amount of seed crystals. When there are more seed crystals the capacity for growth is larger, and that causes the decrease in supersaturation, and so the peaks of growth rate and nucleation rate are both decreased. Figure 3-1 shows the concentration versus time at the very beginning of the process. It shows that for different seed loading ratio, the concentration for larger seed loading ratio case decreases faster than smaller seed loading ratio one. Figure 3-5 shows crystal mass versus time. Dash line is for nuclei crystal and solid line is for seed crystal. Since the

nuclei are undesired, Figure 3-5 shows that the process with higher seed loading has better performance. Based on this observation, we want to determine the relationship between seed loading and the performance of the process. From the work of Kubota and coworkers there is an ideal-growth line to determine "ideal growth". In the next part we want to produce seed charts for both real system and our dimensionless system to see the features of seed charts. The process seeding conditions for both cases are presented in Table 3-1.

Table 3-1 Process parameters used in case study using Chung's parameters.

Variable	Value
L_0	$100\mu m$
M_{seed}	1kg 5kg 10kg
W	$20\mu m$
$f(L)$	$a(110-L_0)(L_0-90)$ where a is determined by M_{seed}

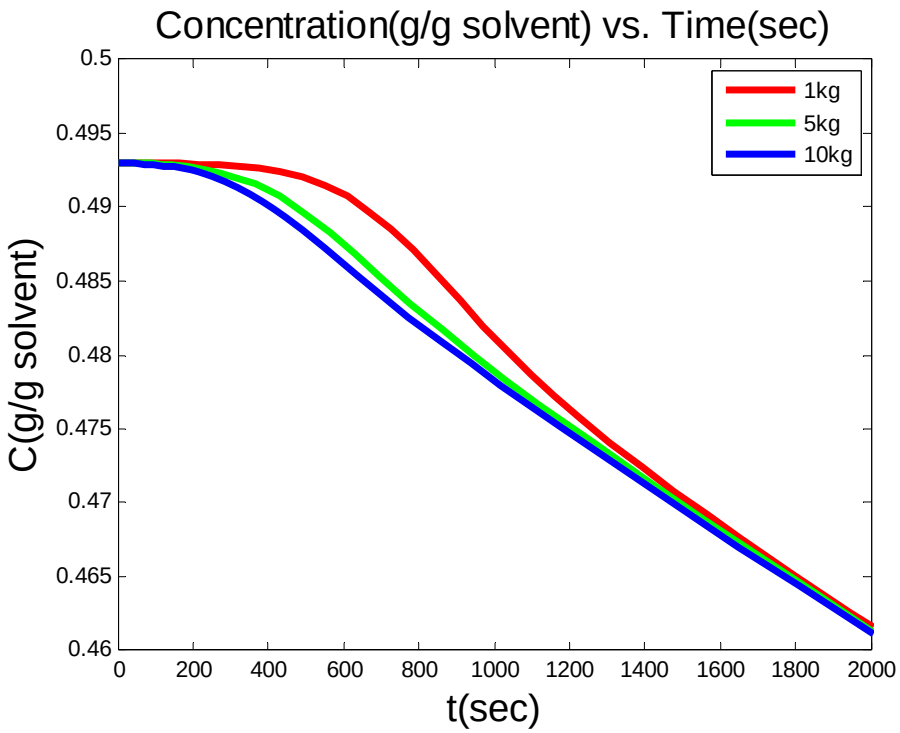

Figure 3-1 Concentration versus time.

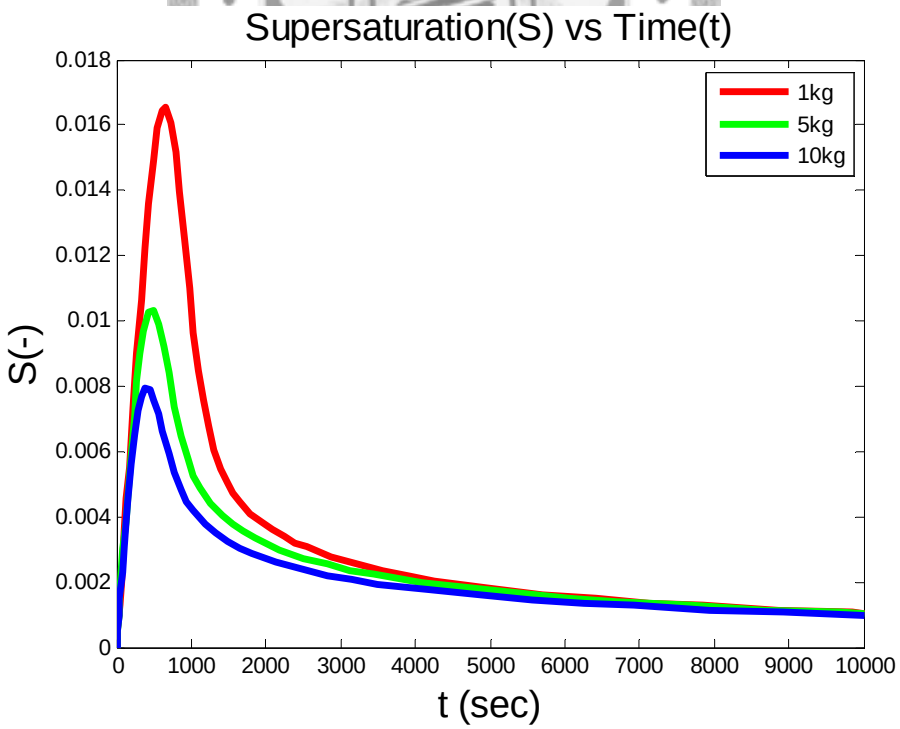

Figure 3-2 Supersaturation versus time.

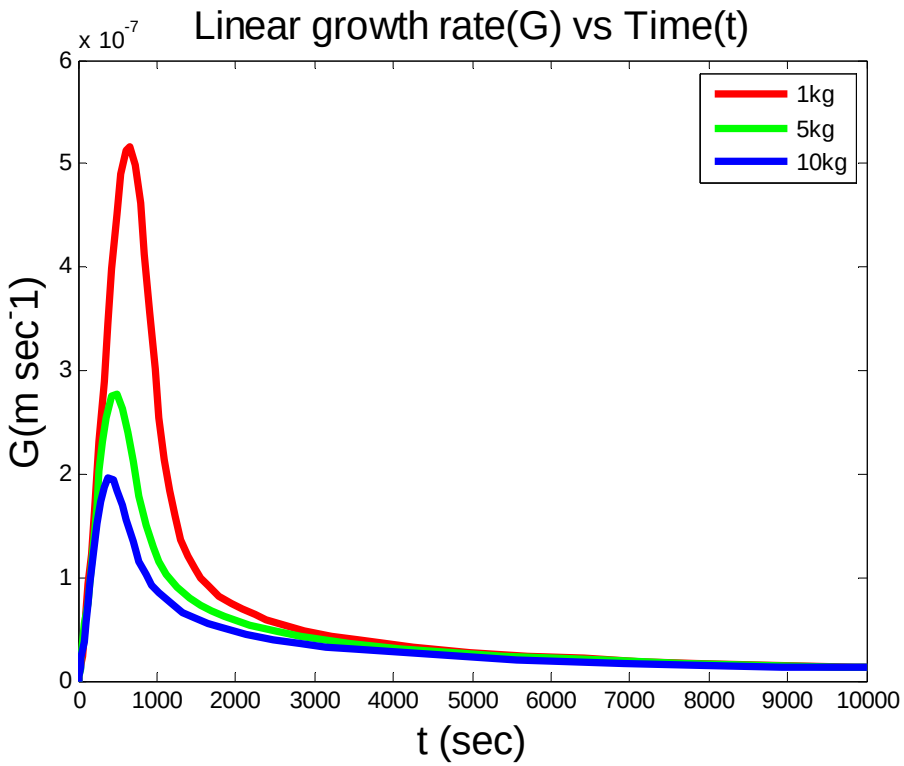

Figure 3-3 Linear growth rate G versus time.

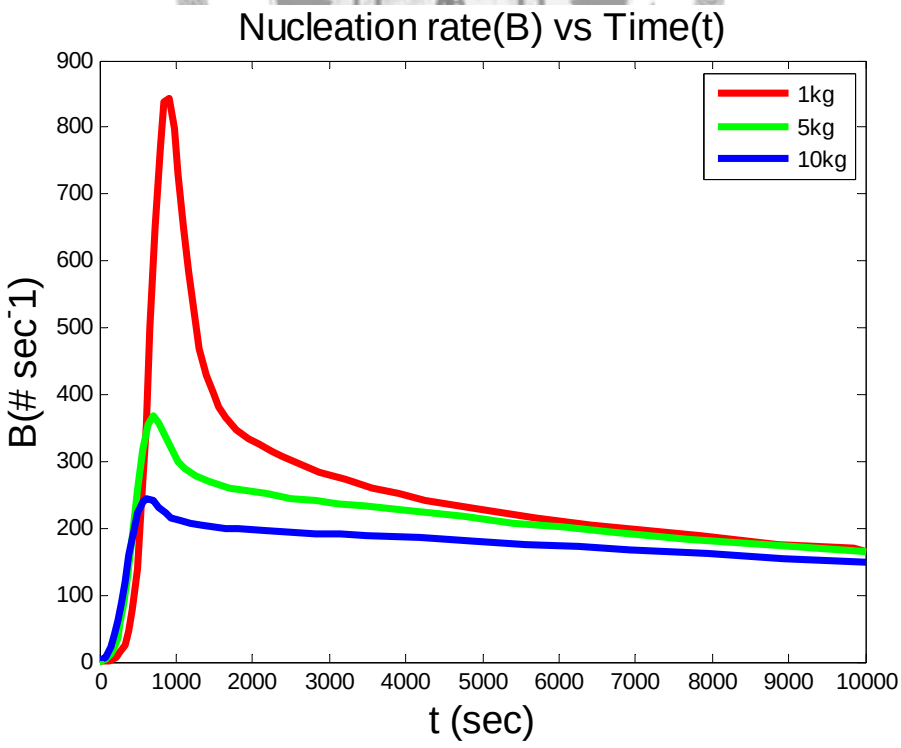

Figure 3-4 Nucleation rate B versus time.

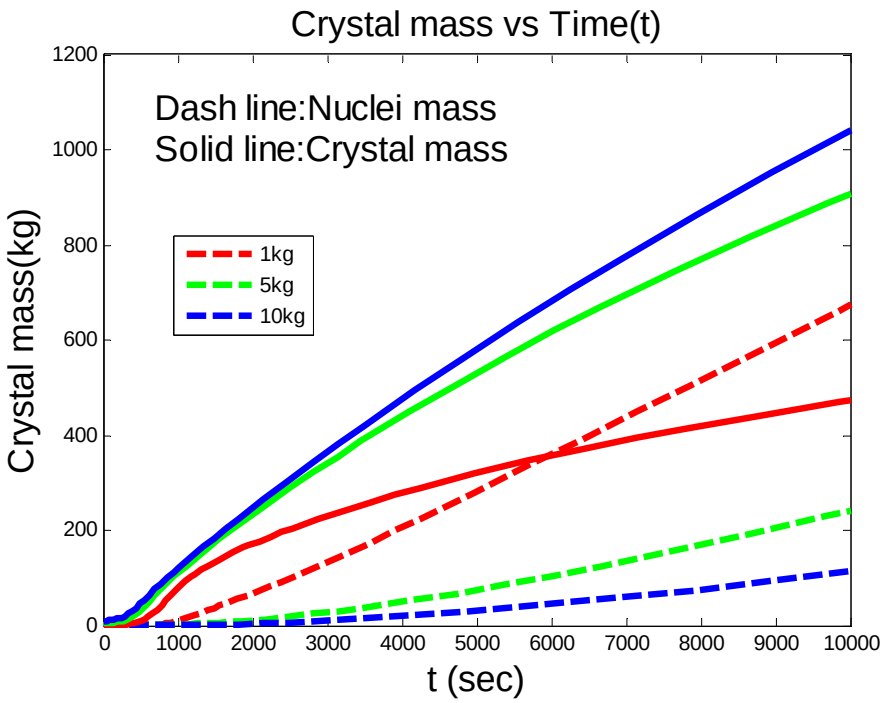

Figure 3-5 Crystal mass versus time

First we observe the effect of seed loading on product crystal size distribution using the dimensionless system. The dimensionless seed mean size x_0' is 0.5, 1.0 and 1.5; Seed mass m_s' is 0.05 and 0.25 respectively, and temperature trajectory is using linear concentration and width w' is 0.5. Figure 3-6 shows the result of different seed loading with different seed mean size x_0'. In Figure 3-6 the product crystal size distribution and volume size distribution have two peaks for both two seed loading m_s', which are a nucleation peak at the left and seed peak at right. Figure 3-6 gives the following conclusions: Larger seed loading reduces the number and mass of nuclei. Product CSD is much better with small seed mean size which is shown in panel (a), but the product mean size of m_s' =0.25 (green line) is smaller compared with m_s'=0.05

(blue line). So we can conclude that seed loading in each case must have a desired value to give a good result without reducing the product mean size too much. Later in this section this desired seed loading is defined as the critical seed loading.

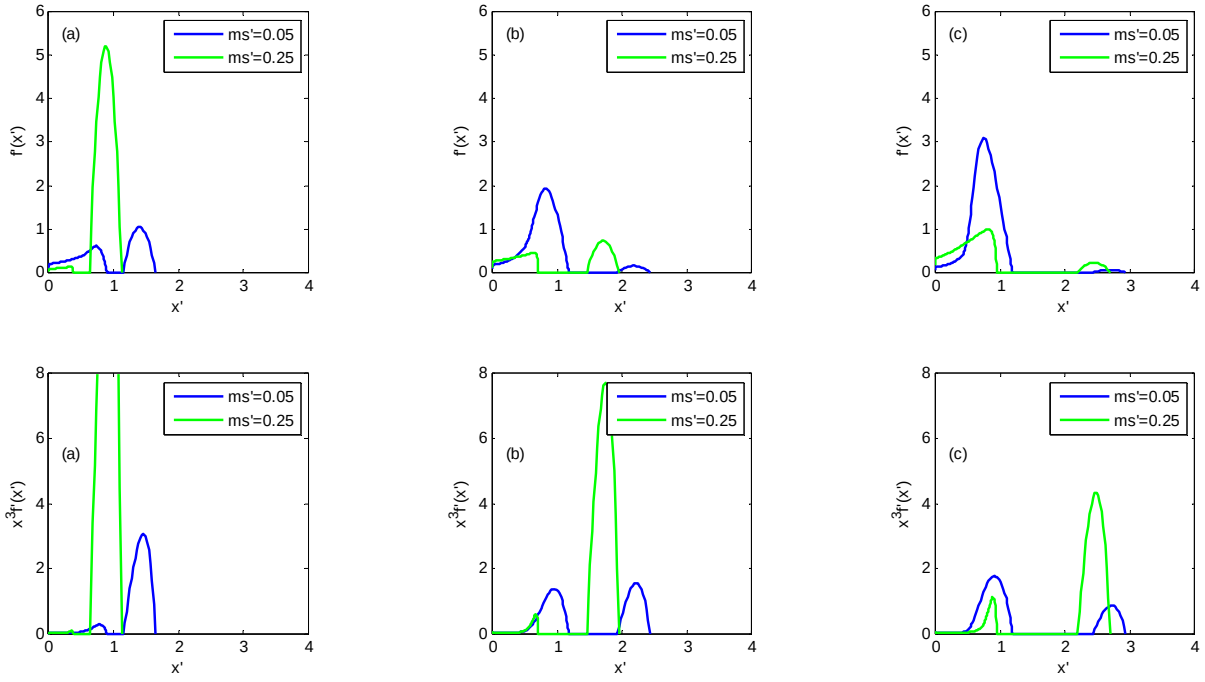

Figure 3-6 Effect of seed loading on product CSD and product VSD. (a) x_0'=0.5 (b) x_0'=1.0 (c) x_0'=1.5. Green line: m_s'=0.25. Blue line: m_s'=0.05.

3.2 Growth rate constraint

In this section we consider a constraint on the growth rate G. If there is a constraint for a maximum value of the growth rate G_{max}, then the result of optimizing the temperature trajectory would be different. The following Figure shows the effect of two different constraints for growth rate using optimal trajectory, and the objective function is to minimize the third moment of nuclei in the end of process. Seeding

conditions are: m_s'=0.05, x_0'=1.0 and w'=0.1. The two constraints are 1.5 times the constant growth rate and 2.0 times constant growth rate, where constant growth rate is defined as a constant value of G that would achieve the desired production rate in the given batch time. Comparing the three cases in Figure 3-7 we find that the growth rate trajectory does not change until the very end of the process. For this particular objective function, which is to minimize nuclei mass in the end, it is still suggested that growth rate peak should be at the very end of process.

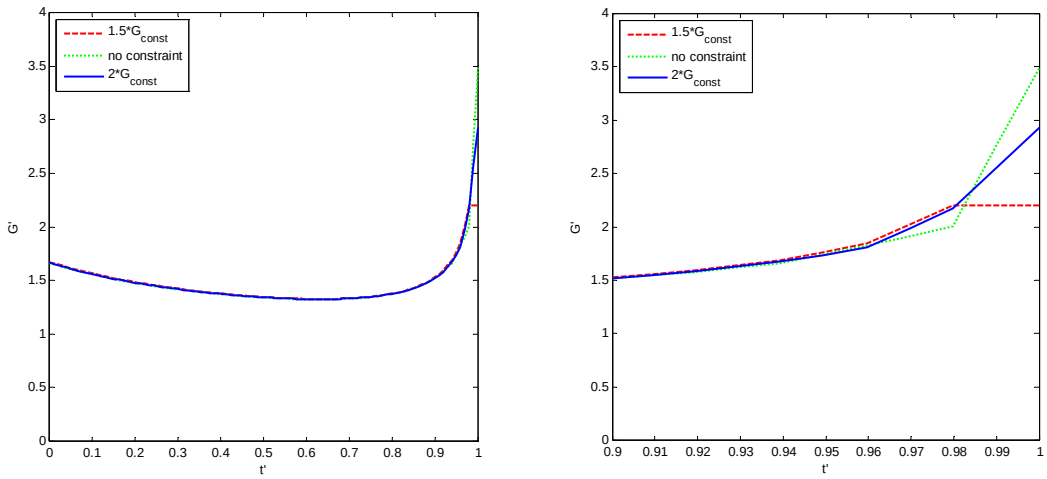

Figure 3-7 Adding a constraint for growth rate. Right hand side Figure is the zoom-in for left hand side Figure.

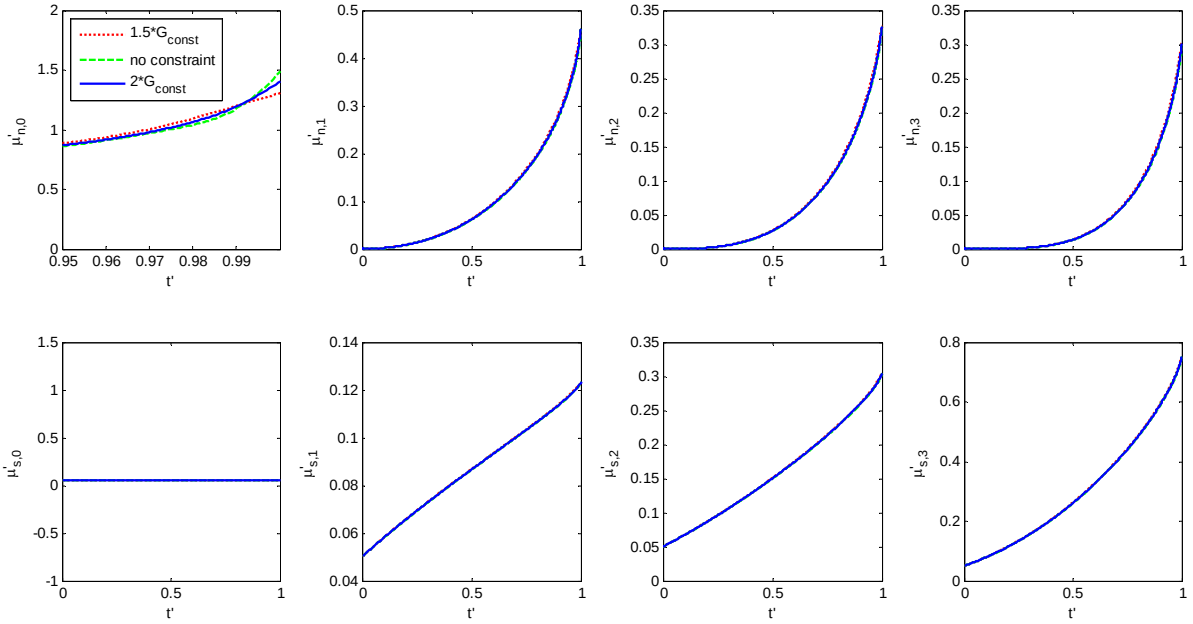

Figure 3-8 The moments plots for adding G constraint.

Figure 3-8 shows the moment plots for the cases with a constraint and the case with no constraint. From upper-left corner Figure we observe that total number of nuclei in the end of process are different compared to three different conditions of G. With the added constraint total number of nuclei in the end is decreasing due to the decrease of growth peak in the end. However, both 1.5 times and 2.0 times G_{const} have almost the same product crystal size distribution and product volume size distribution, indicating that these two constraint do not have significant influences on the product quality.

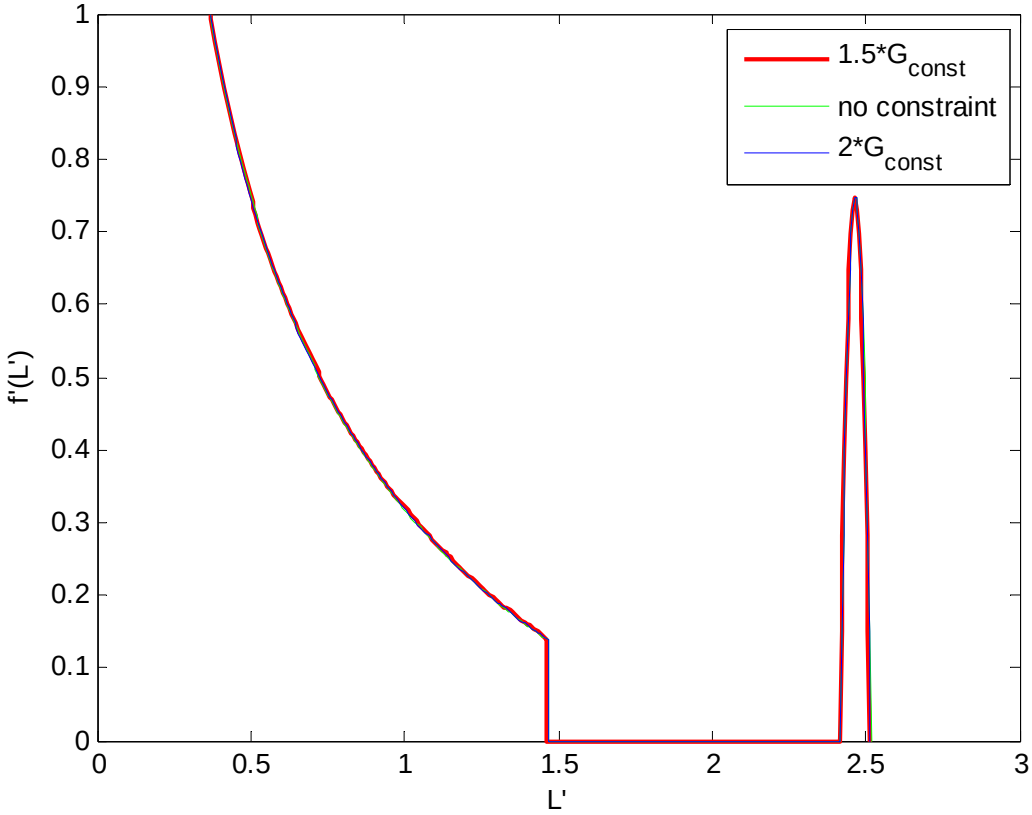

Figure 3-9 Product crystal size distribution

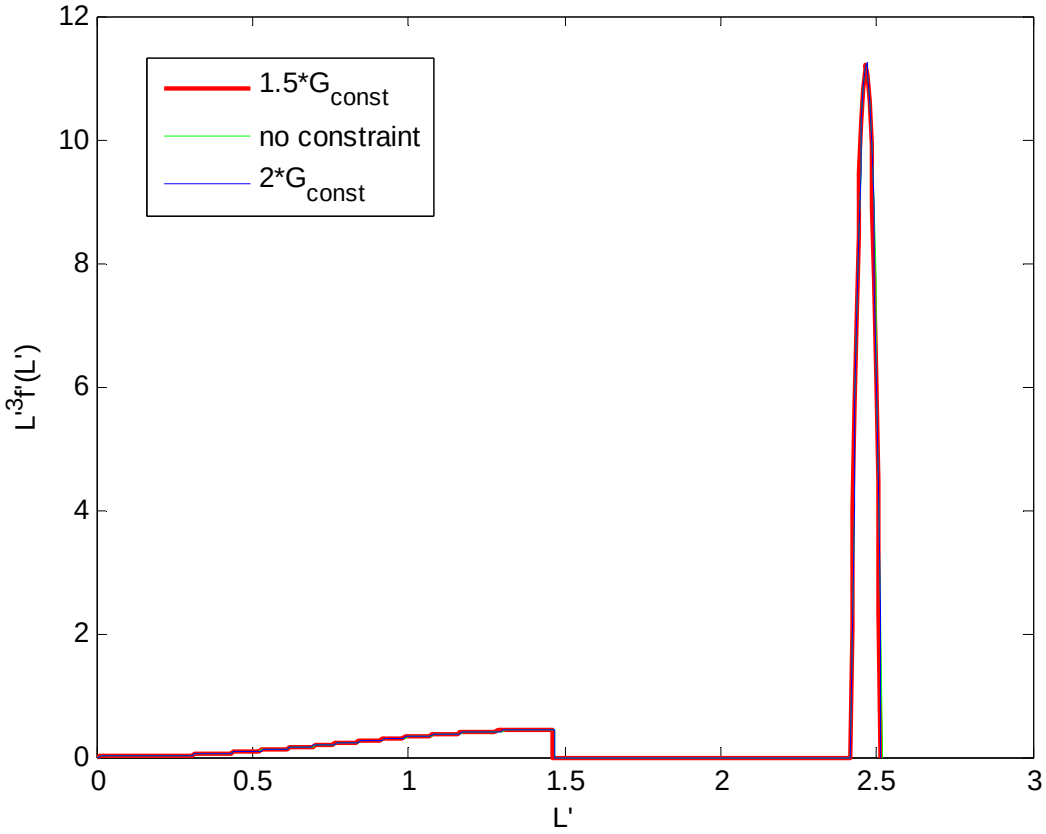

Figure 3-10 Product volume size distribution

4 Analytical expressions of critical seed loading ratio

4.1 Overview

In this chapter we want to predict the nuclei fraction in the end ξ, which is defined as:

$$\xi = \frac{\mu_{3,n}(t_f)}{\mu_{3,T}(t_f)} \tag{4-1}$$

Ant further we want to determine the relationship between C_s^* and x_0' analytically. Mullin and Nyvlt in 1971 published a concentration trajectory for seeded batch crystallization. Here we briefly repeat their derivation. They made the assumption that nucleation does not affect the material balance and the growth rate is a constant independent of time and crystal size, so that gives the expression for monodisperse seeds as a function of time:

$$x(t) = x_0 + Gt \tag{4-2}$$

And by the assumption that G is constant

$$\mu_3(t) = n_0 (x_0 + Gt)^3 \tag{4-3}$$

where n_0 is the number of seed crystals per unit volume of suspension. At the beginning of the batch,

$$m_s = \rho_c k_v \mu_3(0) = \rho_c k_v n_0 x_0^3 \tag{4-4}$$

Then

$$n_0 = \frac{m_s}{\rho_c k_v x_0^3} \tag{4-5}$$

$$\mu_3(t) = \frac{m_s}{\rho_c k_v x_0^3}(x_0 + Gt)^3 \tag{4-6}$$

Finally the concentration at the end of the batch:

$$C_0 - C_f = m_s \left(\left(1 + \frac{Gt_f}{x_0} \right)^3 - 1 \right) \tag{4-7}$$

We can use above results to approximately determine the nucleated mass if the nucleated mass is small. Suppose that only seed crystals contribute to the material balance. Then we can solve for the growth rate G as a function of the average seed size and total seed mass:

$$G = \left(\left(\left(\frac{C_0 - C_f}{m_s} \right) + 1 \right)^{\frac{1}{3}} - 1 \right) \frac{x_0}{t_f} = a \frac{x_0}{t_f} \tag{4-8}$$

Where

$$a = \left(\left(\left(\frac{C_0 - C_f}{m_s} \right) + 1 \right)^{\frac{1}{3}} - 1 \right) \tag{4-9}$$

Recall the definition of nucleation rate B:

$$B = k_B G^{\gamma} \mu_3^j \tag{4-10}$$

Here we discuss two values of j. If j=0 and G is a constant, we can simplify

the ODE set from Equation 2-13 to get the following expression:

$$\mu_{3,n} = 6k_B G^{3+\gamma} \int_0^{t_f}\int_0^{t}\int_0^{t}\int_0^{t} dtdtdtdt = \frac{k_B}{4} G^{3+\gamma} t_f^4 \tag{4-11}$$

From the definition of ξ in Equation 4-1 we can get the expression for the third moment of nuclei in the end of process.

$$\mu_{3,n} = \xi\left(\frac{m_s + (C_0 - C_f)}{\rho_c k_v}\right) \tag{4-12}$$

Combine with Equation 4-9 and 4-10,

$$\mu_{3,n} = \xi\left(\frac{m_s + (C_0 - C_f)}{\rho_c k_v}\right) = \frac{k_B G^{3+\gamma} t_f^4}{4} \tag{4-13}$$

$$\left(\frac{m_s + (C_0 - C_f)}{\rho_c k_v}\right) = \frac{k_B}{4\xi}\left[a\frac{x_0}{t_f}\right]^{3+\gamma} t_f^4 \tag{4-14}$$

Once given seed mass and seed size m_s and x_0, initial and final concentration C_0 and C_f, and batch time t_f with known ρ_c and k_v we can calculate the third moment of nuclei in the end $\mu_{3,n}(t_f)$ along with nuclei fraction in the end ξ.

If j=1:

$$B = k_B G^{\gamma} \mu_3 = k_B G^{\gamma} n_0^3 (x_0 + Gt)^3 \tag{4-15}$$

Then the third moment of nuclei in the end can be calculated,

$$\mu_{3,n} = 6k_B G^{3+\gamma} n_0^3 \int_0^{t_f}\int_0^t\int_0^t\int_0^t (x_0 + Gt)^3 \, dtdtdtdt \tag{4-16}$$

And integrate Equation 4-16 one get:

$$\mu_{3,n} = 6k_B G^{3+\gamma} x_0^3 t_f^4 n_0^3 \left(\frac{1}{840}a^3 + \frac{1}{120}a^2 + \frac{1}{40}a + \frac{1}{24}\right) \tag{4-17}$$

Substitute the relation of n_0 from Equation 4-5 into Equation 4-17:

$$\mu_{3,n} = \frac{6k_B G^{3+\gamma} t_f^4 m_S}{\rho k_v}\left(\frac{1}{840}a^3 + \frac{1}{120}a^2 + \frac{1}{40}a + \frac{1}{24}\right) \tag{4-18}$$

If given needed parameters, we can calculate $\mu_{3,n}(t_f)$ and ξ. Next we change the above relations into dimensionless expressions:

$$x_0 = x_0' \times \bar{G} t_f = x_0' t_f \left(k_B \bar{\mu}_3^{j-1} t_f^4\right)^{\frac{-1}{\gamma+3}} \tag{4-19}$$

So G becomes:

$$G = a\frac{x_0}{t_f} = a x_0' \left(k_B \bar{\mu}_3^{j-1} t_f^4\right)^{\frac{-1}{\gamma+3}} \tag{4-20}$$

The expression for G' is derived:

$$G = a\frac{x_0}{t_f} = a x_0' \bar{G} \Rightarrow G' = \frac{G}{\bar{G}} = a x_0' \tag{4-21}$$

Substitute Equation 4-20 into Equation 4-13 (note that in this case j=0).

$$\mu_{3,n} = \xi\left(\frac{m_s + \left(C_0 - C_f\right)}{\rho_c k_v}\right) = \frac{k_B G^{3+\gamma} t_f^4}{4} = \frac{1}{4}(a x_0')^{3+\gamma} \bar{\mu}_3 \tag{4-22}$$

Further rearrange the left hand side of Equation 4-22:

$$\mu_{3,n} = \xi\left(\frac{m_s + \left(C_0 - C_f\right)}{\rho_c k_v}\right) = \xi\left(\frac{\left(m_s^{'} + 1\right)\left(C_0 - C_f\right)}{\rho_c k_v}\right) = \xi\left(m_s^{'} + 1\right)\bar{\mu}_3 \qquad (4\text{-}23)$$

Then combine with Equation 4-22 and 4-23 it becomes:

$$\xi\left(m_s^{'} + 1\right) = \frac{1}{4}(ax_0^{'})^{3+\gamma} \qquad (4\text{-}24)$$

Where a is also derived with dimensionless groups and a is a function of $m_s^{'}$.

$$a = \left(\left(\left(\frac{C_0 - C_f}{m_s}\right) + 1\right)^{\frac{1}{3}} - 1\right) = \left[\left(m_s^{'-1} + 1\right)^{\frac{1}{3}} - 1\right] \qquad (4\text{-}25)$$

Here derive again with j=1. Start from Equation 4-18 we get:

$$\xi\left(m_s^{'} + 1\right) = 6m_s^{'}\eta(a)(ax_0^{'})^{3+\gamma} \qquad (4\text{-}26)$$

Where η is:

$$\eta(a) = \left(\frac{1}{840}a^3 + \frac{1}{120}a^2 + \frac{1}{40}a + \frac{1}{24}\right) \qquad (4\text{-}27)$$

Derivation results are summarized in Table 4-1.

Table 4-1 Summary of derivations for different values of j

j	Equation for $\mu_{3,n}(t)$	Relationship of $m_s^{'}$ vs. $x_0^{'}$
0	$\mu_{3,n} = \xi\left(\frac{m_s + \left(C_0 - C_f\right)}{\rho_c k_v}\right) = \frac{k_B G^{3+\gamma} t_f^4}{4}$	$\xi\left(m_s^{'} + 1\right) = \frac{1}{4}(ax_0^{'})^{3+\gamma}$
1	$\mu_{3,n} = \frac{6k_B G^{3+\gamma} t_f^4 m_S}{\rho k_v}\left(\frac{1}{840}a^3 + \frac{1}{120}a^2 + \frac{1}{40}a + \frac{1}{24}\right)$	$\xi\left(m_s^{'} + 1\right) = 6m_s^{'}\eta(ax_0^{'})^{3+\gamma}$

4.2 Simulation result

Figures show the resulting critical seed loading values using the analytical expression and simulation for different j values using dimensionless system. In Figure 4-1 kinetic parameters are: γ=3.0 & j=1. From Figure 4-1 the simulation result using the optimal trajectory has a slightly smaller seed loading ratio C_s^* than the analytical result throughout the whole range of x_0'. However, in Figure 4-2 the analytical expression fits very well with constant growth rate trajectory. This is also not surprising because they are based on the same assumption, namely that the growth rate is constant. As seed loading ratio is larger, the nucleation rate B is suppressed so as the seed loading ratio reaches the critical value, B is suppressed to almost zero. Considering with these two above assumptions, constant growth rate trajectory with critical seed loading ratio may be the best fitting for analytical expression. As for Figure 4-3 and 4-4 (where j=0), the analytical expression also fits well with constant G trajectory, and the chart for the optimal growth rate has a has slightly smaller seed loading than analytical one. Table 4-6 gives the correlation results of dimensionless growth rate G' versus time t'. For small seed mean size (which is 0.5 and red lines here) the deviation is relatively large, but as large seed size (1.0 and 1.5), the correlations are good from Figure 4-6. In conclusion, the analytical expressions for

γ=3.0 with both j=1 and j=0 cases are good, and the correlation for growth rate G' is also good. In Figure 4-5 we also find out for the range of x_0' from 0.1 to about 2.0, the two lines for j=0 and j=1 gradually approach each other and overlap at about x_0'=2.0, i.e., the differences of critical seed loading ratio for j=0 and j=1 are large at small seed mean size but small at large seed mean size.

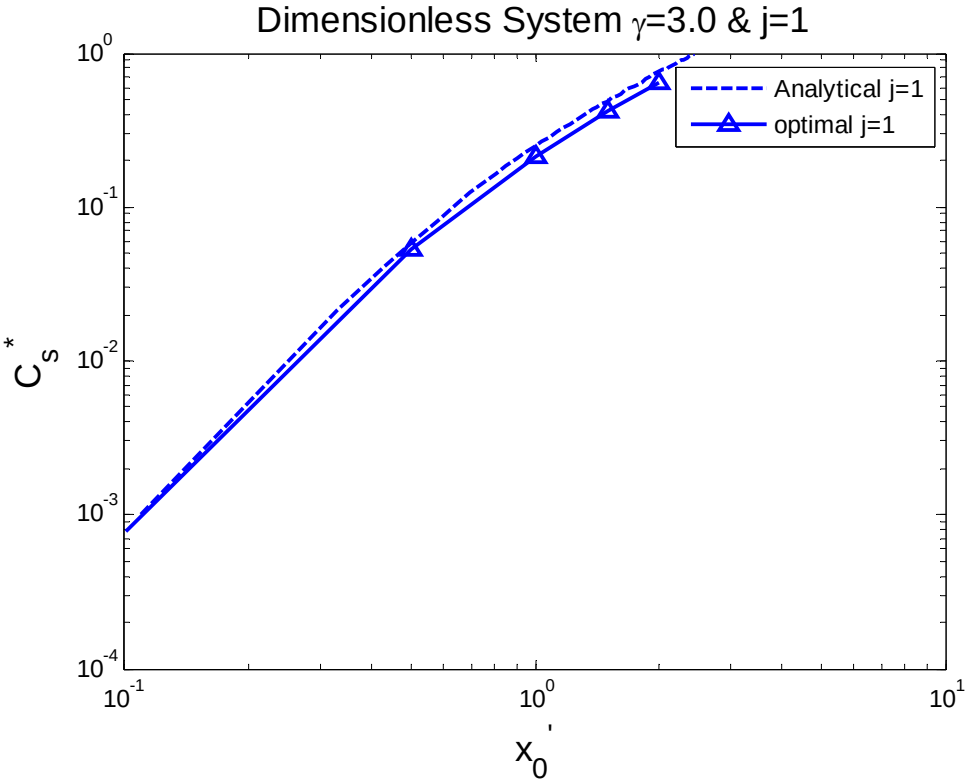

Figure 4-1 Comparison between analytical and simulation result with γ=3 & j=1.

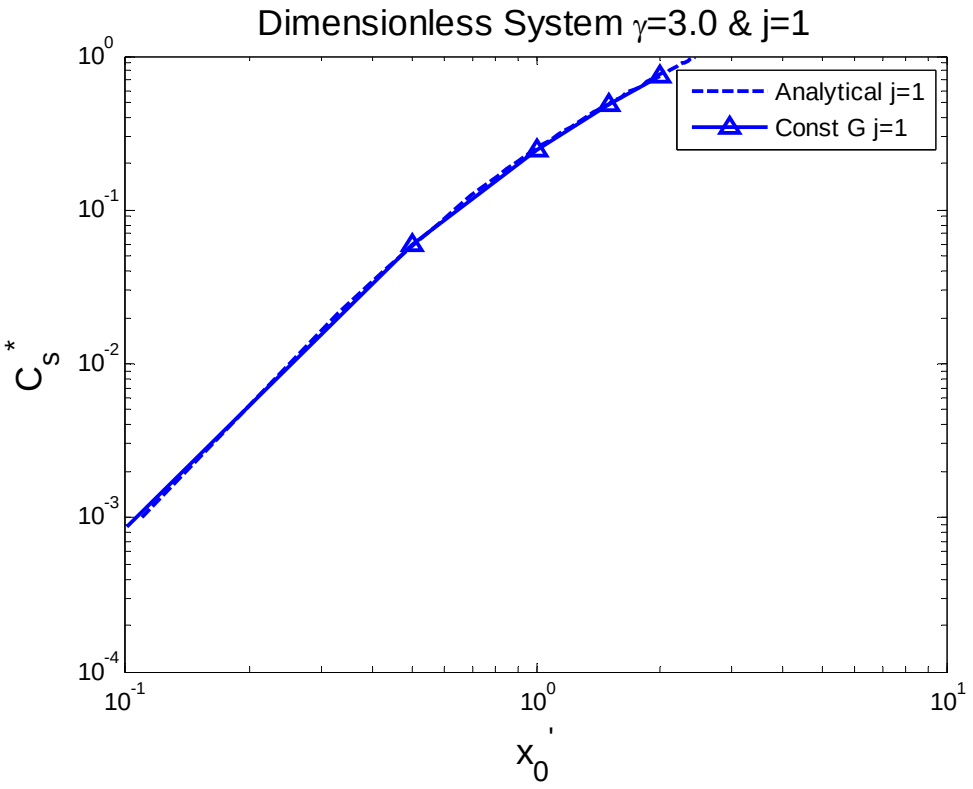

Figure 4-2 Comparison between analytical and simulation results with *γ=3* & *j*=1.

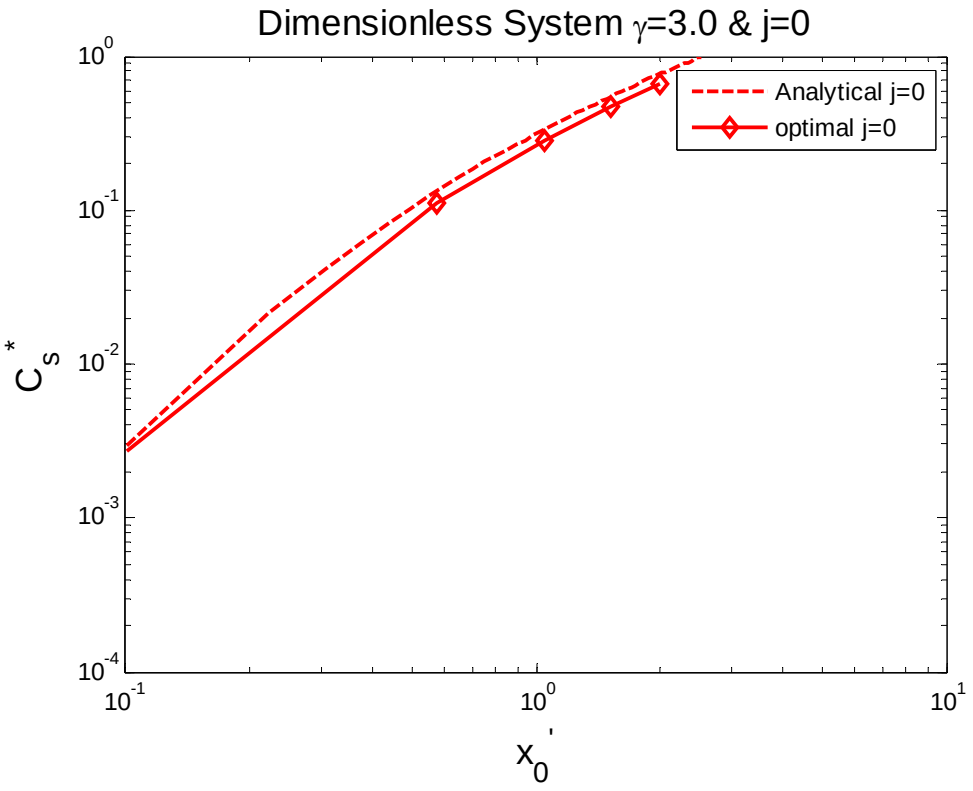

Figure 4-3 Comparison between analytical and simulation with *γ=3* & *j*=0.

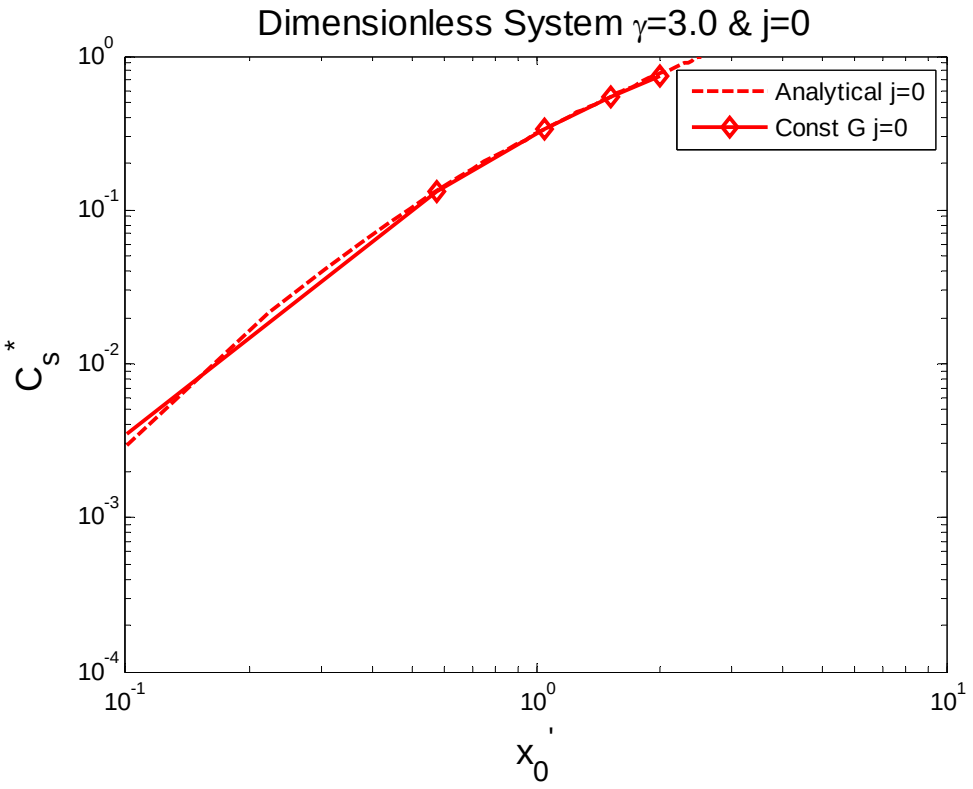

Figure 4-4 Comparison between analytical and simulation with $\gamma=3$ & $j=0$.

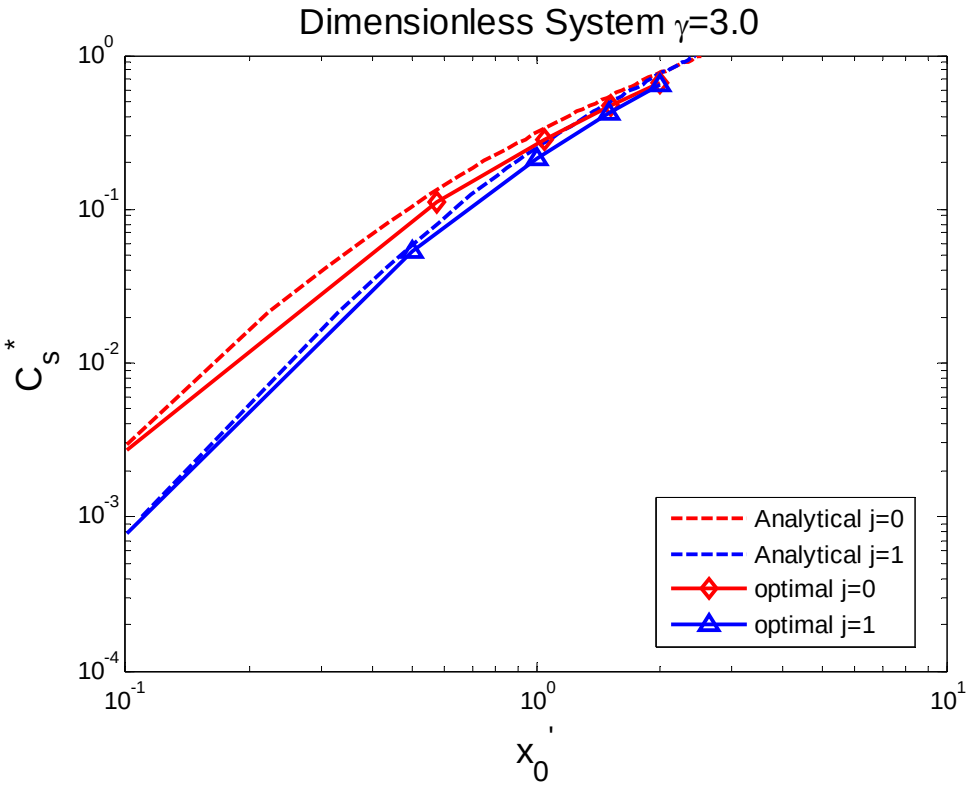

Figure 4-5 Comparison of different j between analytical and simulation result

Table 4-2 Comparison between analytical growth rate and simulation growth rate

x_0'	m_s'	a	G'(analytical)	G'(simulation)
0.5	0.0601	1.6031	0.8015	0.8483
1.0	0.2492	0.7114	0.7114	0.7192
1.5	0.4905	0.4484	0.6726	0.6717

5 Seed Charts

5.1 Overview

A typical seed chart is plotted to see the trends of normalized product volume mean size L_p/L_s versus seed loading ratio C_s, and also can be used to determine the critical seed loading ratio C_s^*. Subscripts p and s of L represent for product and seed crystal. The main purpose of the normalized product volume mean size is to show product quality. When L_p/L_s is larger this means that the product size is also larger. Seed loading ratio and volume mean size are defined by

$$C_S = \frac{W_s}{W_{th}} \tag{5-1}$$

$$L = \frac{\sum_{i=1}^{N} w_i l_i}{\sum_{i=1}^{N} w_i} = \frac{\sum_{i=1}^{N} n_i l_i^4}{\sum_{i=1}^{N} n_i l_i^3} \tag{5-2}$$

Where W_s is mass of seed (kg) and W_{th} is theoretical crystal yield (kg). The value of W_{th} can be calculated or determined by its definition

$$W_{th} = w(C_i - C_f) \tag{5-3}$$

Here w is mass of solvent water (kg). C_i and C_f are the initial solution concentration (kg solute/ kg solvent water) and final concentration (kg solute/ kg solvent water) in the crystallizer respectively.

Note that Equation 5-2 assume a discrete crystal size distribution function N is

the total number of discrete lengths and n is the total amount of each discrete length crystal. Equation 5-2 is used to correlate experimental data. In our simulation we simply use the following relation of L since L is the volume mean size.

$$L = \frac{\mu_4}{\mu_3} \tag{5-4}$$

5.2 Seed chart and empirical Equation

In several publications about batch seeded crystallization mentioned in the introduction section, the authors plotted seed charts using experimental data for different systems. For real crystal systems, we use kinetic parameters in two papers, published by Chung et al. (potassium nitrite from water) and one by Sarkar et al. (potassium sulfate from water) to produce seed charts, which are shown below. Notice that the expression for nucleation rate here for the potassium nitrate system is slightly different from definition in Chapter 2,

$$B = k_b S^b \mu_3 \tag{5-5}$$

Definition for supersaturation is:

$$S = \frac{C - C_{sat}}{C_{sat}} \tag{5-6}$$

And definition of growth rate is the same:

$$G = k_g S^b \tag{5-7}$$

Table 5-1 Kinetic parameters from Chung et al.

Variable	Name	Value	Units
m_{solv}	mass of solvent	7.57×10^{3}	kg
ρ_c	density of crystal	2.11×10^{3}	kg/m^3
k_v	volumetric shape factor	1	dimensionless
k_b	nucleation parameter	4.6401×10^{11}	#/m^3 s
b	nucleation parameter	1.78	dimensionless
k_g	growth parameter	1.1612×10^{-4}	m/s
g	growth parameter	1.32	dimensionless

For the system of Sarkar et al, the expressions for nucleation and growth rate are as follows.

$$B = k_b e^{-E_b/RT} S^b \mu_3 \tag{5-8}$$

$$G = k_g e^{-E_g/RT} S^b \tag{5-9}$$

Here the definition of supersaturation is the same for Chung's process.

Table 5-2 Kinetic parameters by Sarkar's.

Variable	Name	Value	Units
m_{solv}	mass of solvent	3000	kg
ρ_c	density of crystal	2.66×10^{-12}	$g/\mu m^3$
k_v	volumetric shape factor	1.5	dimensionless
k_b	nucleation parameter	285	$\#/\mu m^3\ s$
b	nucleation parameter	2.25	dimensionless
k_g	growth parameter	1.44×10^{8}	$\mu m/s$
g	growth parameter	1.5	dimensionless
E_g/R	growth rate activation energy divided by gas constant	4859	K
E_b/R	nucleation rate activation energy divided by gas constant	7517	K

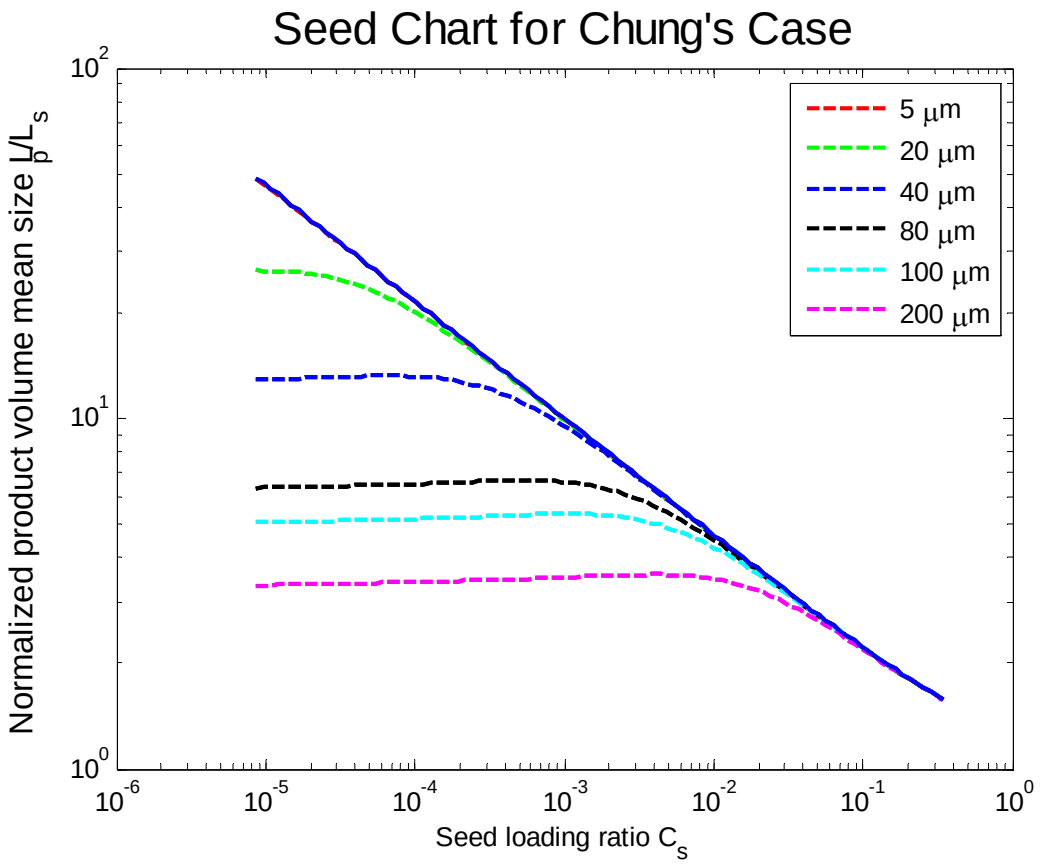

Figure 5-1 Seed Chart using Chung's kinetic parameters.

The seed chart for Chung's case is shown in Figure 5-7. The product volume mean size versus the seed loading ratio is plotted for six different seed sizes. The blue solid line in the Figure is called the ideal-growth line, and the assumptions for this line are as follows: No change in the number of crystals, no generation of new crystals and no change in crystal shape. Note that in Figure 5-7 the line for seed volume mean size of 5μm overlaps the ideal growth line because critical seed loading ratio C_s^* for 5μm is smaller than 10^{-5}. With those assumptions and a mass balance one can derive an analytical expression for the ideal-growth line. Because of the assumption that

there is no nucleation, all the crystals in the solution are grown from the seeds, and from the assumptions crystal shape is the same, we can substitute product volume mean size L_p for seed volume mean size L_s and add a term for the theoretical crystal yield W_{th} on seed mass W_s in the following expression,

$$\frac{W_s}{\alpha\rho_c L_S^3} = \frac{W_s + W_{th}}{\alpha\rho_c L_P^3} \tag{5-10}$$

Then through rearrangement of the above Equation we get,

$$\frac{L_P}{L_S} = \left(\frac{1+C_S}{C_S}\right)^{(1/3)} \tag{5-11}$$

Equation 5-11 is the "ideal-growth" line. When C_s is smaller than about 0.1,

$$1 + C_S \approx 1 \tag{5-12}$$

And the Equation 5-11 for ideal-growth line becomes,

$$\frac{L_P}{L_S} = C_S^{-(1/3)} \tag{5-13}$$

So the slope of ideal-growth line in seed chart is about -1/3 on logarithmic paper. The seed chart for Sarkar's case is shown in Figure 5-8.

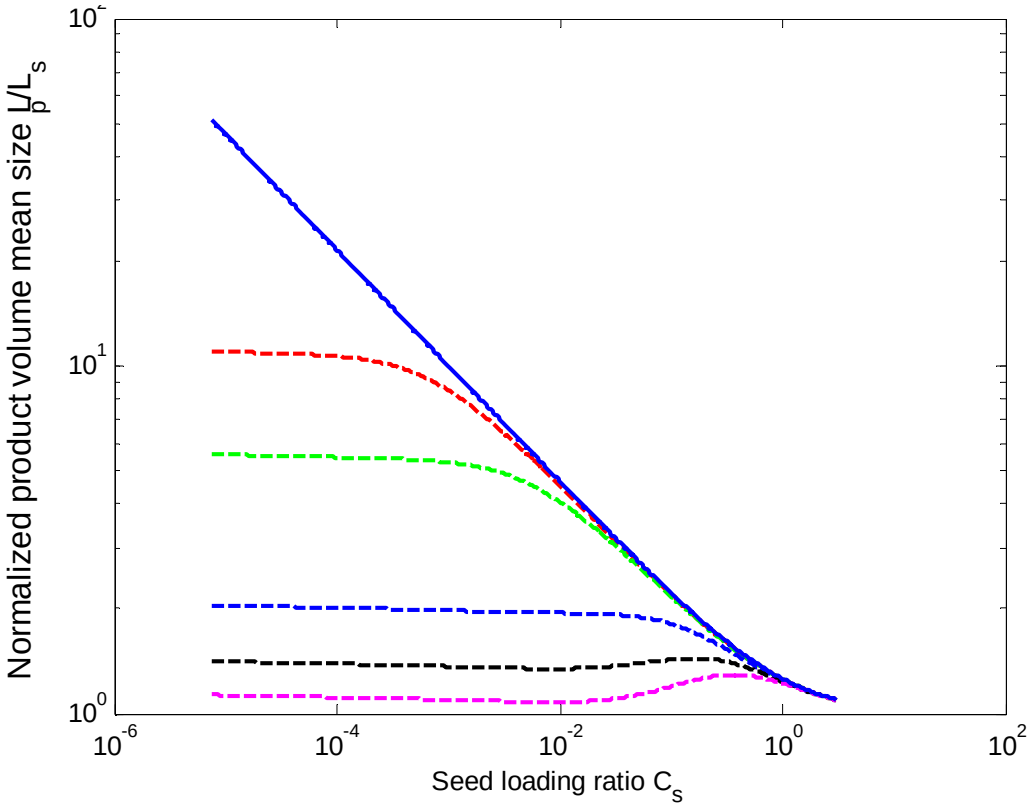

Figure 5-2 Seed Chart using Sarkar's kinetic parameters.

There is a phenomenon that the lines for different seed sizes in both the KNO_3 and K_2SO_4 process are almost flat before C_s reaches critical C_s*. The reason may be a tradeoff between number of seed crystals and seed size. As the number of seed crystals increases, more solute from solution grows on seed crystals (and less on nucleated crystal), however more seeds means less amount of solute for each single crystal to grow, so at the end of process the products are smaller, so L_p/L_s is smaller.

The chart for determining empirical Equation is plotted as below.

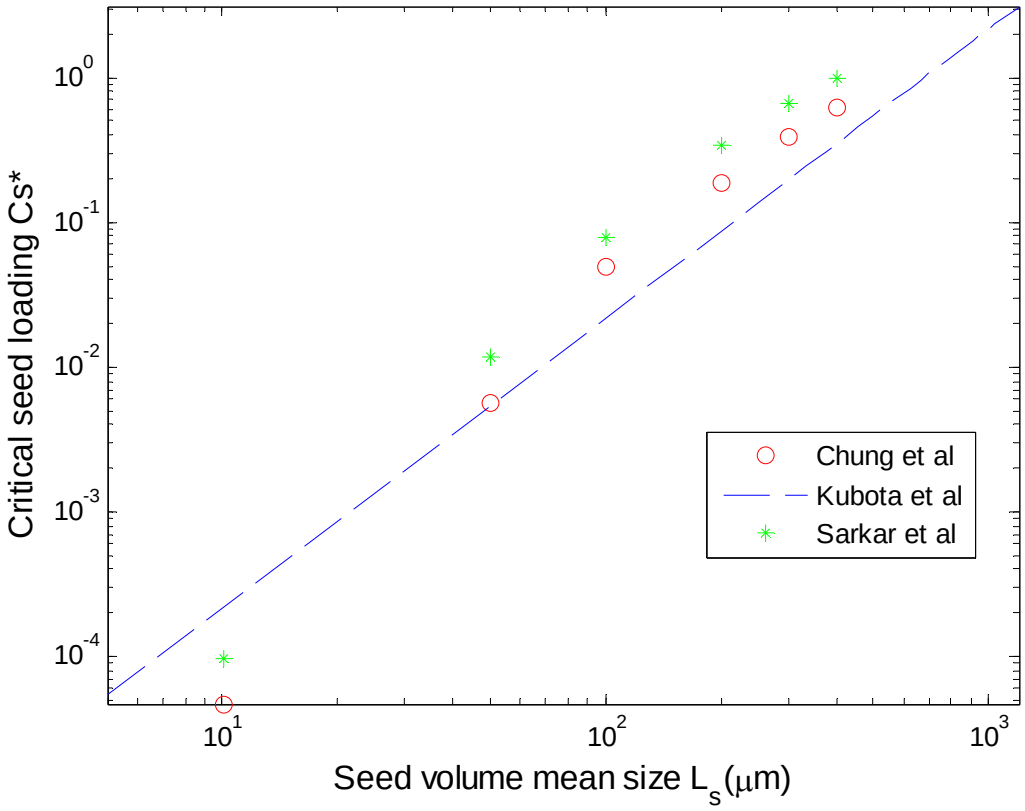

Figure 5-3 Comparison of different crystal system.

Figure 5-9 shows that the simulation results (red circles and green stars in the Figure) for both Chung's and Sarkar's case are close to the empirical correlation of Kubota et al. For Kubota's case, the empirical correlation is:

$$C_S^* = 2.17 \times 10^{-6} L_S^2 \qquad (5\text{-}14)$$

And the units of L_s in Equation 5-14 are μm. But minor deviations from their prediction may occur on the parameters of each system, the parameters are different from case to case. Thus we conclude that the parameters of empirical Equation for different kinds of crystal system should be a range of values depending on different kinetic parameters of crystal systems, and we can further analyze such processes

using the dimensionless system.

For both KNO_3 case and K_2SO_4 case we use MATLAB built-in curve-fitting toolbox to determine an empirical Equation. For KNO_3 case:

$$C_S^* = 1.98\times10^{-5} L_S^{1.728} \tag{5-15}$$

For K_2SO_4 case:

$$C_S^* = 6.24\times10^{-5} L_S^{1.618} \tag{5-16}$$

For the dimensionless system (γ=1.5 and j=1):

$$C_S^{*'} = 0.2808\times x_0^{'1.61} \tag{5-17}$$

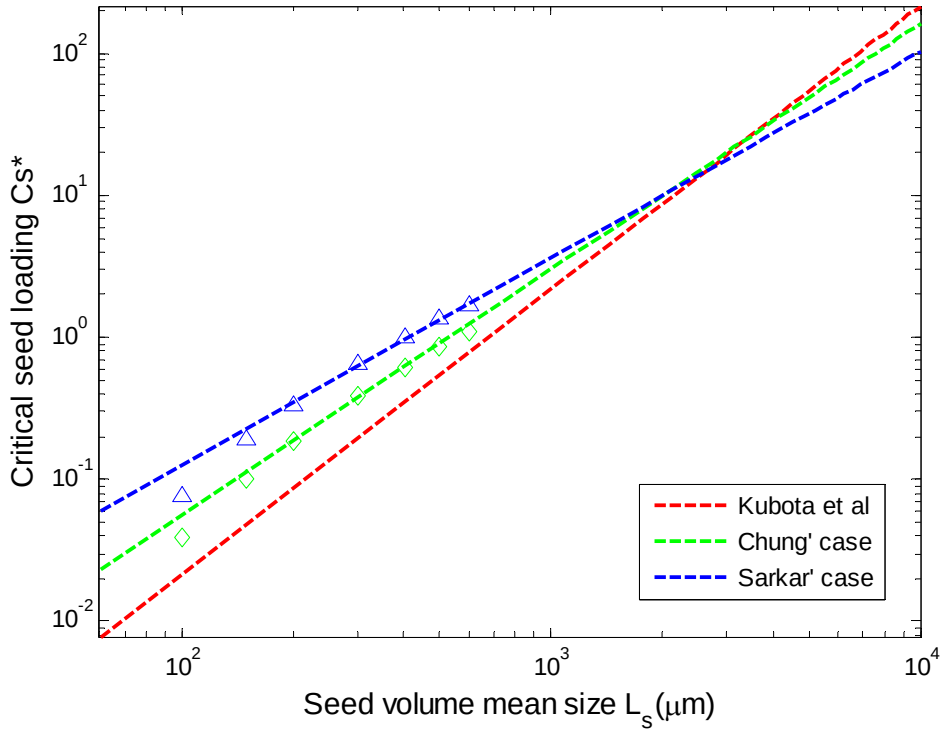

Figure 5-4 Correlation of different real crystal system

Figure 5-10 shows the correlation results of three different real crystal systems. For the dimensionless system, we set the value of γ, which is nucleation parameter b

over growth parameter g, to be 1.5, which is very close to value of K_2SO_4 system (1.45). The exponent on the average seed size for both dimensionless and K_2SO_4 case is similar.

Other information about the curve fitting is provided in Tables 5-3 to 5-5. For those Tables the expressions for the empirical equation is defined as:

$$C_S^* = aL_S^b \tag{5-18}$$

Table 5-3 Fitting results for Chung's case.

Description	**Remark**
95 % confidence bounds of *a*	(8.16e-007, 3.886e-005)
95 % confidence bounds of *b*	(1.565, 1.892)
Adjusted R-square	0.9985
RMSE	0.009791

Table 5-4 Fitting results for Sarkar's case.

Description	**Remark**
95 % confidence bounds of *a*	(-2.172e-005, 0.0001465)
95 % confidence bounds of *b*	(1.388, 1.848)
Adjusted R-square	0.9965
RMSE	0.02417

Table 5-5 Fitting results for dimensionless system with γ=1.5.

Description	**Remark**
95 % confidence bounds of *a*	(0.2413,0.3203)
95 % confidence bounds of *b*	(1.376, 1.846)
Adjusted R-square	0.9973
RMSE	0.0180

There is an important issue should be discussed: in our simulation we make the arbitrary choice that the criteria of achieving "ideal-growth" is that the nucleated mass

is only 1% of the total at the end of the process. The following two Figures show the effect of choosing a different criterion, using Chung's kinetic parameters. Figure 5-11 shows that the line for 0.01% of nuclei is higher than 1% of nuclei. If we specify a stricter criterion, critical seed loading ratio is larger. Another point is that from Figure 5-12 the influence of different criteria for the product size is much more significant. Table 5-7 is the values of product size over seed size L_p/L_s using two different criteria for different seed size L_s. For the case of L_s equals to 100μm**,** the product size is 153μm for 0.01% of nuclei and 292μm for 1% of nuclei respectively. The reason is that to achieve the stricter criteria a higher seed loading is required, so each seed commonly grow to a smaller size. Note that the dashed line in Figure 5-11 is the empirical Equation determined by Kubota et al. Finally, we decided to use 1% nucleated mass of nuclei as our criteria to determine the ideal growth line because in Figure 5-11 the data for 1% nucleated mass is close to Kubota's correlation and it also seems to be a reasonable choice.

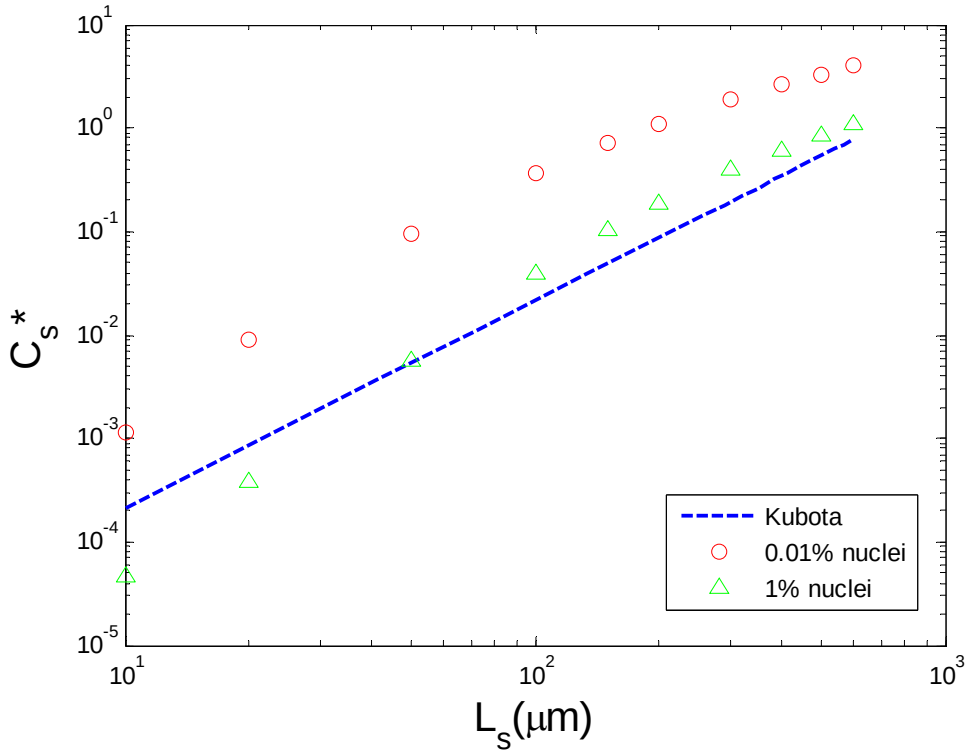

Figure 5-5 Chart for determining empirical Equation

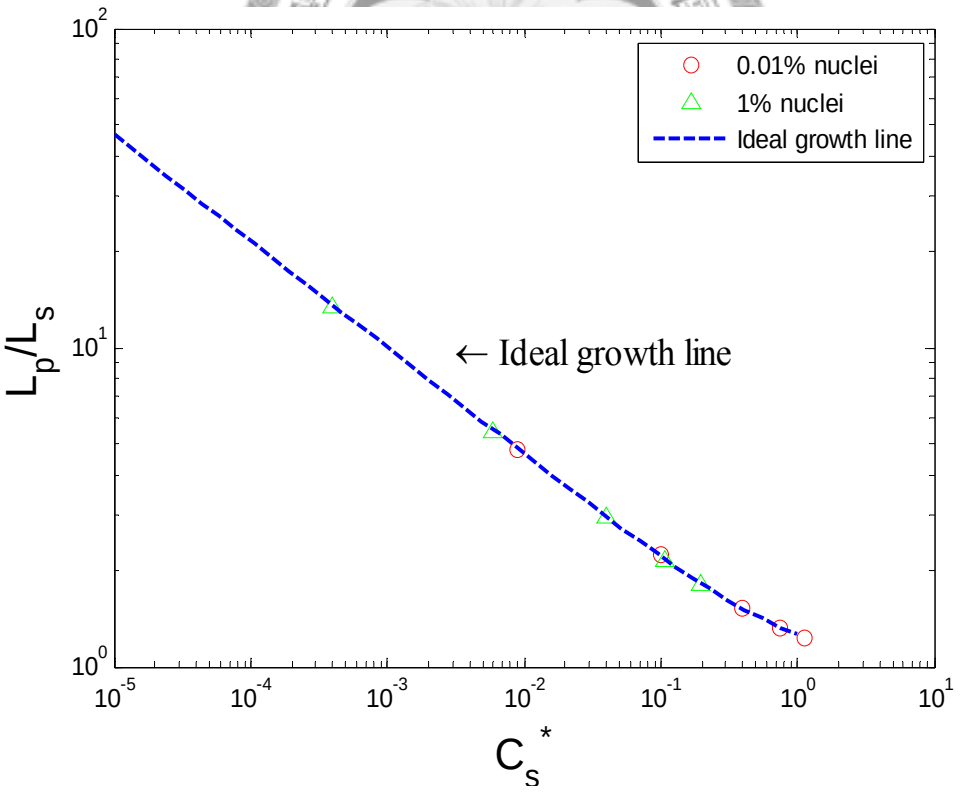

Figure 5-6 Seed Chart for dimensionless system

Table 5-6 L_p/L_s of two different criterion given different seed size L_s.

L_p/L_s	L_s=20μm	L_s=50μm	L_s=100μm	L_s=150μm	L_s=200μm
0.01% of nuclei	4.82	2.23	1.53	1.33	1.24
1% of nuclei	13.47	5.48	2.92	2.16	1.81

The following Figures are seed chart for dimensionless system and Figure for determining empirical Equation.

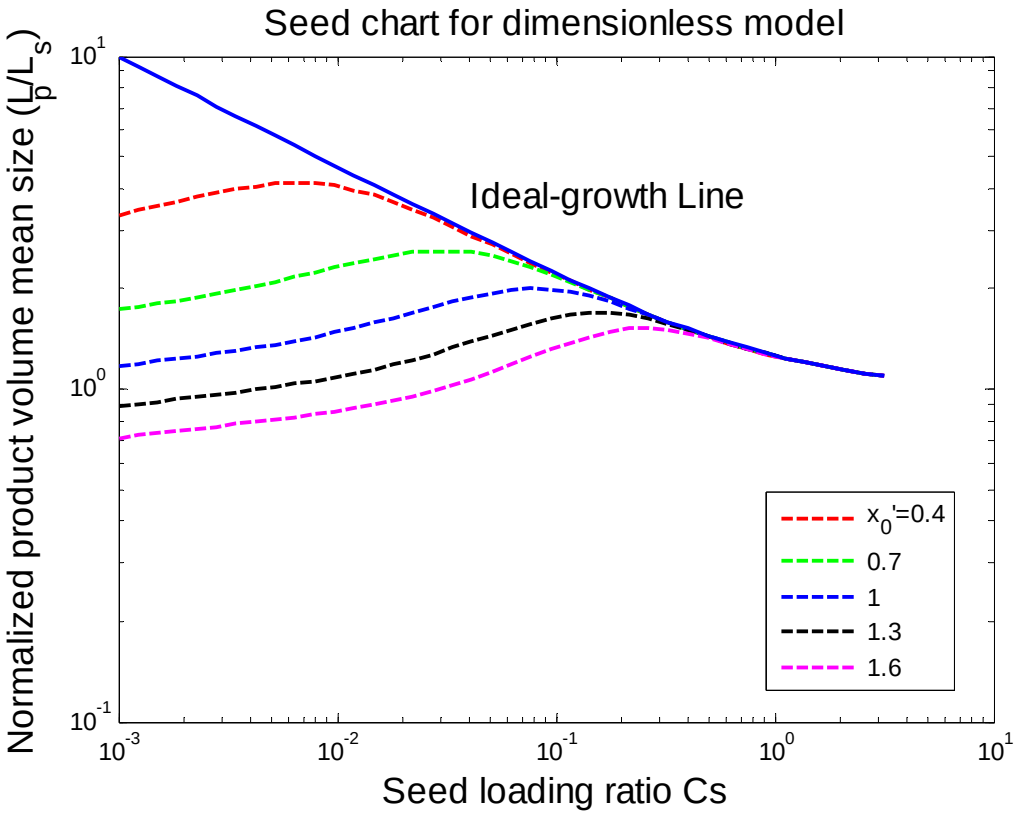

Figure 5-7 Seed chart for cooling crystallization of dimensionless system

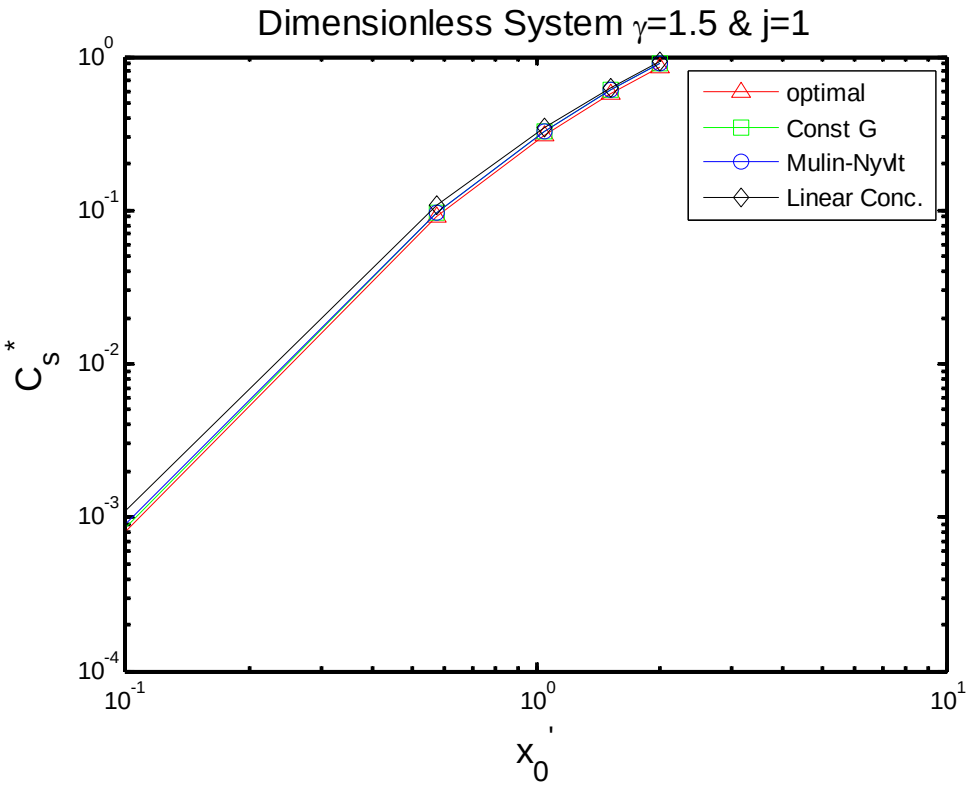

Figure 5-8 C_s* vs. x_0' for dimensionless system (γ=1.5).

Recall that γ is the ratio of nucleation parameter b over growth parameter g. For dimensionless system, we compare four different temperature trajectories in order to see the effect of varying temperature trajectory, which are linear concentration, optimal, Mullin-Nyvlt and constant growth rate trajectories. The results are shown in Figure 5-14. The assumptions of the Mullin-Nyvlt trajectory are: no nucleation and growth rate is constant. Through some derivation (Mullin and Nyvlt, 1971; Ward et al., 2011) the dimensionless mathematical expression of Mullin-Nyvlt trajectory is shown:

$$C'(t') = 1 - \frac{((1+at')^3 - 1)}{((1+a)^3 - 1)} \tag{5-19}$$

where a is given by,

$$a = \left(\frac{1}{m_s' + 1} \right)^{1/3} - 1 \tag{5-20}$$

All four lines in Figure 5-14 are very close, suggesting that as seed loading is increased to the critical value C_s*, the influence of different cooling mode is almost negligible, i.e., the performances are almost the same for four temperature trajectories when seed loading reaches C_s*. As before, with a smaller seed size, a smaller value of C_s* is needed and vice versa.

However, when the figure is reproduced for different values of γ, there is a significant difference. As γ is increases, the difference between the four trajectories becomes larger. For example, when γ is about 1.5 (this value is close to the K_2SO_4 system) the differences among four trajectories are small. But when γ is 3.0 as in Figure 5-15, there is a greater difference among the four trajectories. Recall from definitions of the kinetic Equations,

$$G = k_g S^g \tag{5-21}$$

$$B = k_b S^b \mu_3 \tag{5-22}$$

As the value of γ is larger, the value of b is larger or g is smaller. The value of

supersaturation is smaller than 1.0. So larger b leads to smaller nucleation rate, and smaller g leads to larger crystal growth rate. Generally, if γ is large, the difference between B and G is amplified. From Figure 5-15 we can conclude that large value of γ would amplify the efficiencies of the trajectories.

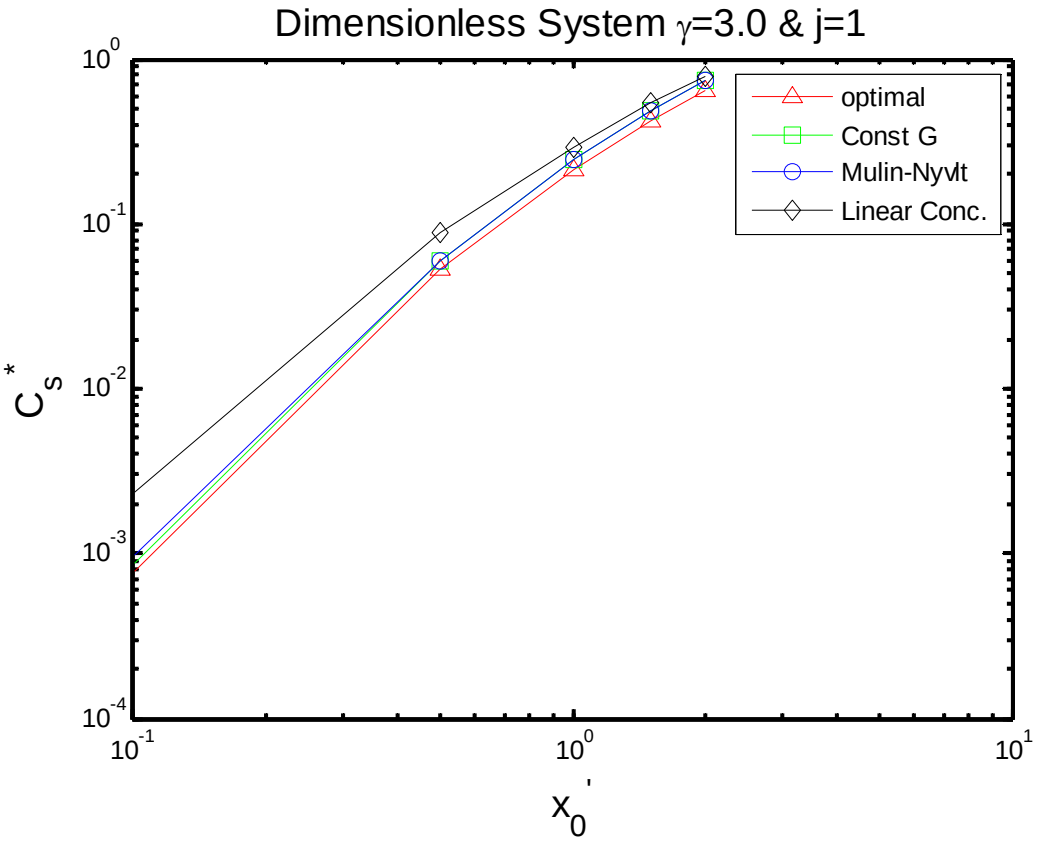

Figure 5-9 C_s* vs. x_0' for dimensionless system (γ=3.0).

Ward et al. in previous publication pointed out among the four trajectories, optimal, constant growth rate, Mullin-Nyvlt and linear concentration, the linear concentration is much worse than the other three, while the constant growth rate and Mullin-Nyvlt are almost as good as the optimal one. Also note that in Figure 5-15 the

trend is the same as reported by Ward et al., i.e., the linear concentration trajectory is worse than the other three.

5.3 Critical seed loading ratio with different kinetic parameters

In this section we want to further find out the influences of kinetic Equation on the critical seed loading ratio. The definition of nucleation rate in dimensionless system is:

$$B = k_b G^{\gamma} \mu_3^{\,j} \tag{5-23}$$

Figure 5-16 gives the critical seed loading ratio as a function of seed mean size x_0' for γ=3.0 and j=0. Compared with Figure 5-15 where j=1, when x_0' is small, the critical seed loading ratio is larger when j=0. But when x_0' is large, the critical seed loading ratio C_s^* is almost the same for all j values and all trajectories, indicating that C_s^* is not affected by trajectory and kinetic exponent parameters when seed size x_0' is large enough. For all different j values, the value of C_s^* is much larger for linear concentration trajectory than the others at small x_0', and slightly higher at middle and large x_0', which means that linear concentration gives a worse result than the other three trajectories. In Figure 5-17 when j=2, C_s^* is slightly larger than the one in Figure 5-15 where j=1. In overall comparison from j=0 to j=2, when x_0' is small (around 0.1) there is a difference in C_s^* value, but when x_0' is larger, C_s^* are almost the same.

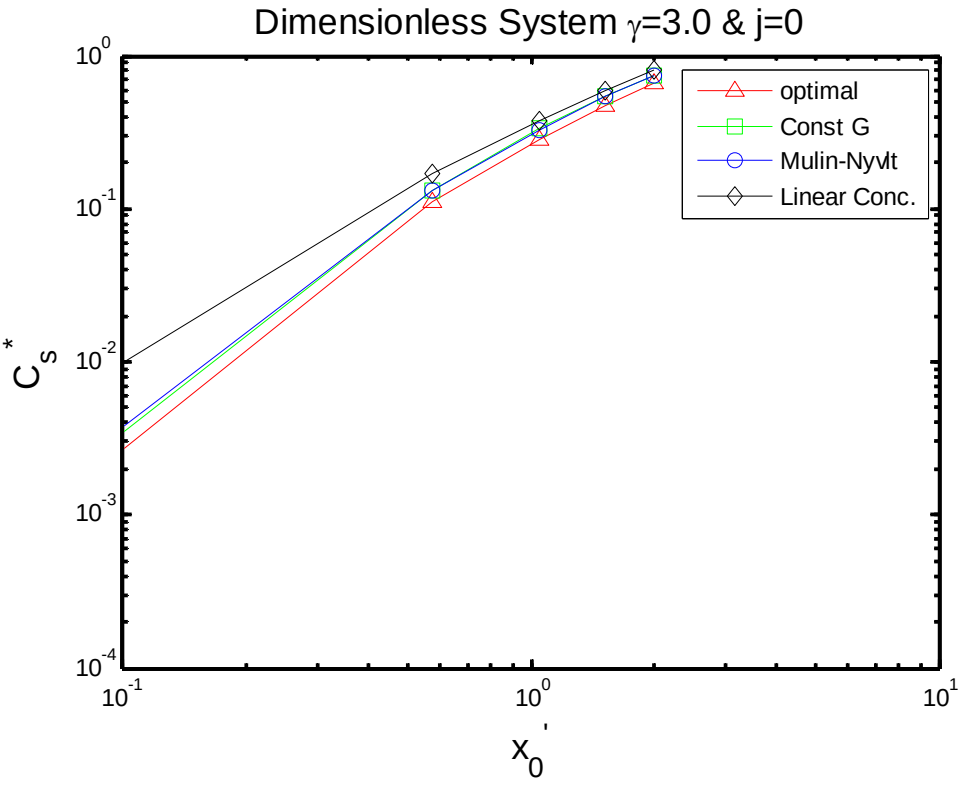

Figure 5-10 C_s* vs. x_0' for dimensionless system (γ=3.0 and j=0).

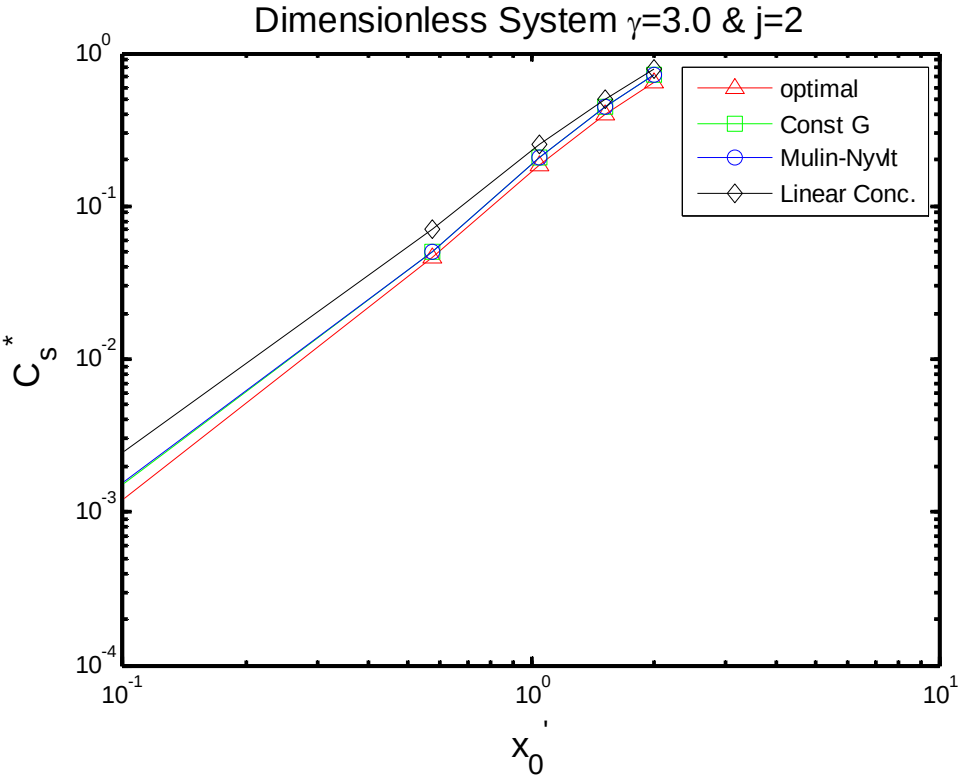

Figure 5-11 C_s* vs. x_0' for dimensionless system (γ=3.0 and j=2).

6 Notion of critical seed surface area

Lung-Somarriba et al. proposed a variable called critical surface area S_c to determine seeding policy. They concluded that the concept of critical surface area S_c can be used to design seeding for small seed size. They further stated that large size of seed would lead to attrition of crystals and reduction of growth rate. In other words, the concept of critical surface area S_c can be used only for small seed size.

Here we want to investigate the idea of using the critical surface area to design seeding policy. Note that in this chapter all Figures are plotted for the dimensionless system. Figure 6-1 shows contour of different moments of seed crystals at that achieve the criteria of 1% of nuclei and 5% of nuclei with γ=3.0 and j=1. In Figure 6-1 we plot for sufficiently large range of seed properties (seed size and seed mass) and fix seed width to be the value of 0.1, using the linear concentration trajectory. In Figure 6-1 there is a critical value for the first moment of seed crystal μ_1, which is about 0.36 for 1% of nuclei. Green dash line is the critical value.

As seed number mean size L_0 is large, μ_0 should be small in order to keep μ_1 the same. In other words, if L_0 is small, μ_0 should be large. Although seed properties can be specified using above relations, in many cases this will result in far more seeds than necessary. As the points A and B in upper-left corner subFigure in Figure 6-1,

two points are both far away from 1% of nuclei if we specify 1% of nuclei as the criteria, which causes waste in seed crystals and also reduces the final product size as discussed in previous chapter. Another note is that in Figure 6-1 we also find out a critical value for μ_2, and the relationship between S_c and L_0 is analogous to C_s^* vs. L_s. Although critical values of μ_1 and μ_2 may exist, it is not efficient to use this variable as design variable for seeding policy. Note that the average surface area or average mass of seed crystal as a function of seed mean size cannot be used as the variables for seeding policy because here we fix seed CSD to be parabolic distribution, once we decide the seed mean size, the seed average mass and surface area is fixed, as shown in Figure 6-13.

Figure 6-1 to Figure 6-6 are the moments plot for different values of γ and j. The critical values of μ_1 and μ_2 are different from different values of γ and j. And the total crystal surface area versus seed number mean size are plotted in Figure 6-7 to Figure 6-12. Results for the moments contour plots are summarized in Table 6-1. When γ is fixed at 3.0, the value of $\mu_{1,c}$ is largest for j=0, and smallest when j=2 while the value of $\mu_{2,c}$ is largest when j=2 and smallest when j=0. The same trend for different j can be observed when γ is equal to 1.5. For three particular cases the critical values are very large (see Table 6-1), and we do not decide the exact values of them since the seed

number mean size μ_1/μ_0 should be increased to a very large value to get the exact value.

From Figure 6-7 to Figure 6-12, the critical value of total surface area μ_2 is reached until μ_1/μ_0 is larger than 2.0.

In conclusion, it is not recommended to use only critical μ_1 or μ_2 as design variable, instead we keep using two variables, which are seed size and seed mass (or loading ratio) to determine seed condition.

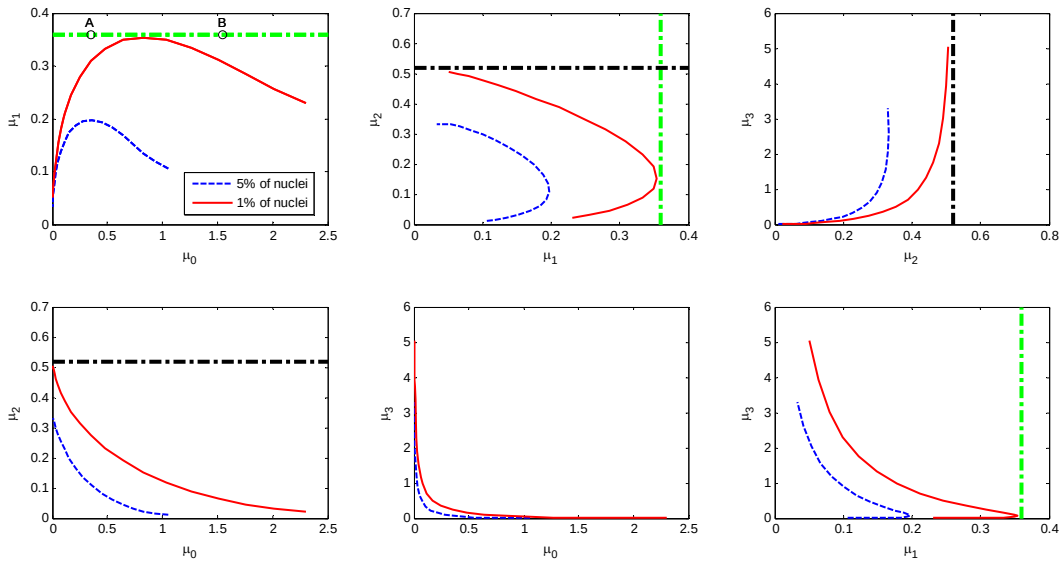

Figure 6-1 Moments contour plot using linear concentration trajectory for dimensionless system γ=3.0 and j=1. Blue dash line is for 5% of nuclei, red solid line is for 1% of nuclei.

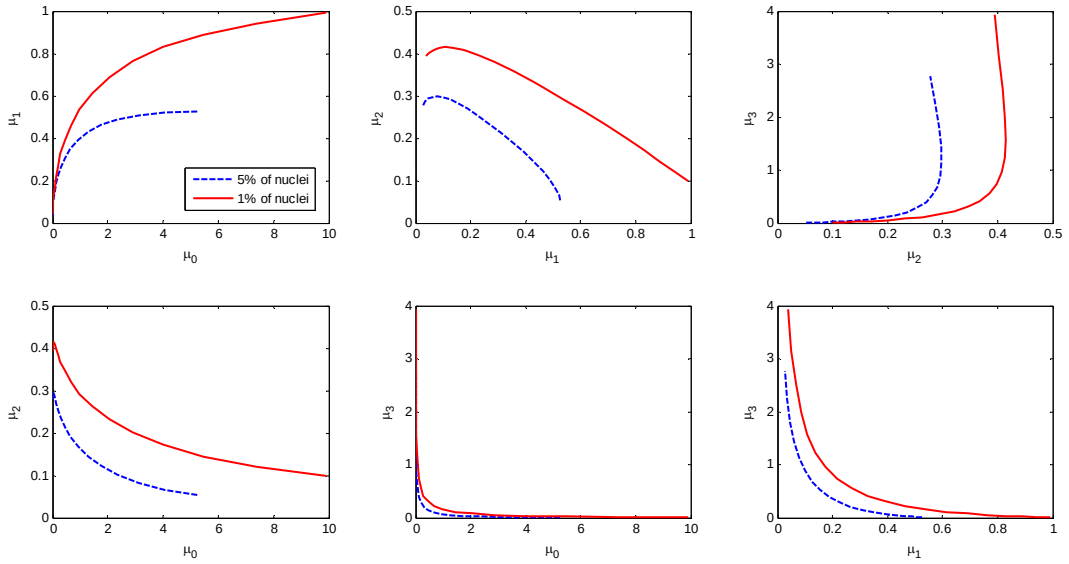

Figure 6-2 Moments contour plot using linear concentration trajectory for dimensionless system γ=3.0 and j=0. Blue dash line is for 5% of nuclei, red solid line is for 1% of nuclei.

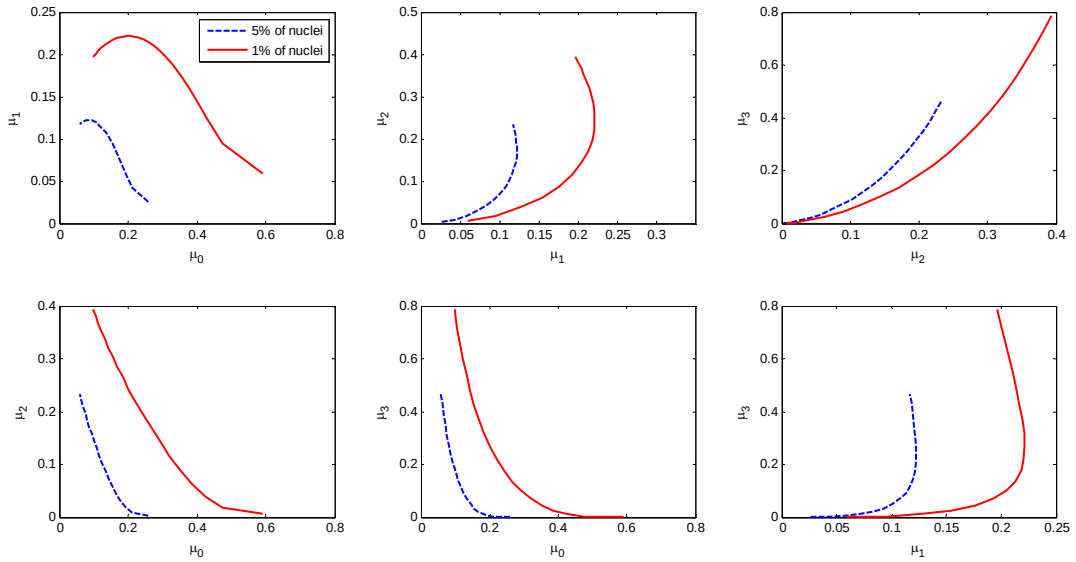

Figure 6-3 Moments contour plot using linear concentration trajectory for dimensionless system γ=3.0 and j=2. Blue dash line is for 5% of nuclei, red solid line is for 1% of nuclei.

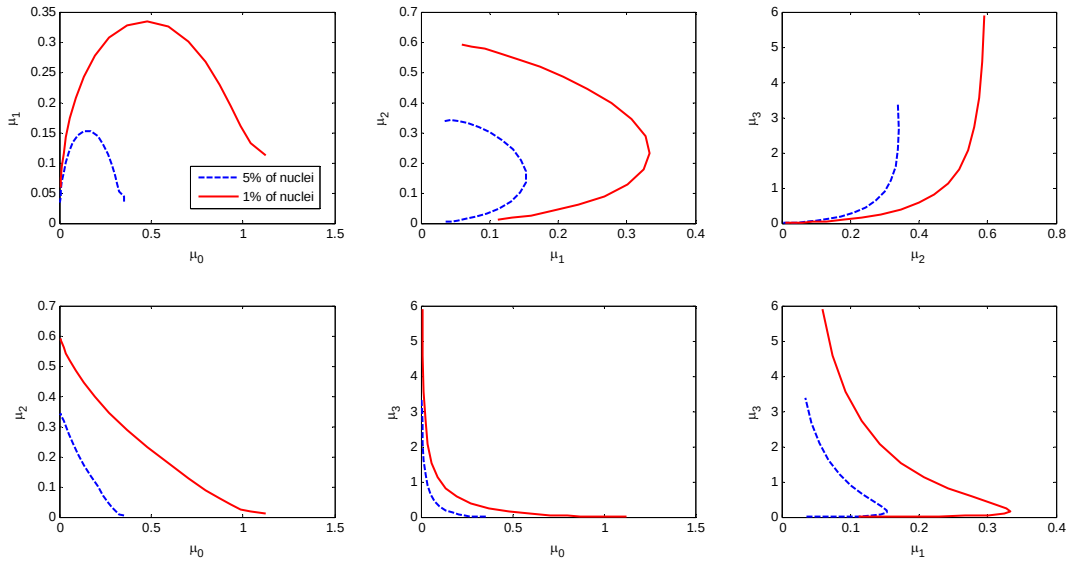

Figure 6-4 Moments contour plot using linear concentration trajectory for dimensionless system γ=1.5 and j=1. Blue dash line is for 5% of nuclei, red solid line is for 1% of nuclei.

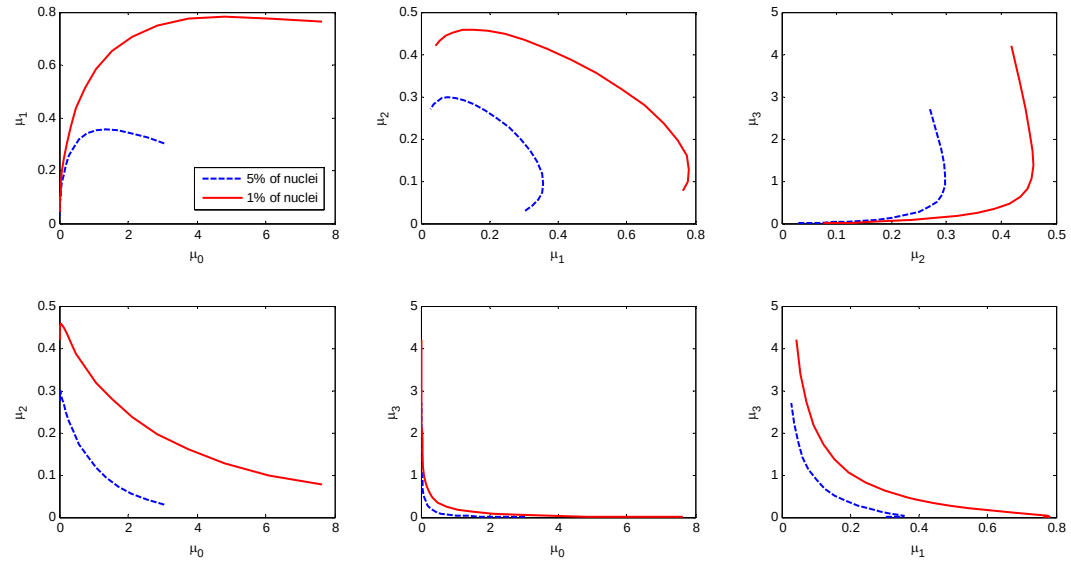

Figure 6-5 Moments contour plot using linear concentration trajectory for dimensionless system γ=1.5 and j=0. Blue dash line is for 5% of nuclei, red solid line is for 1% of nuclei.

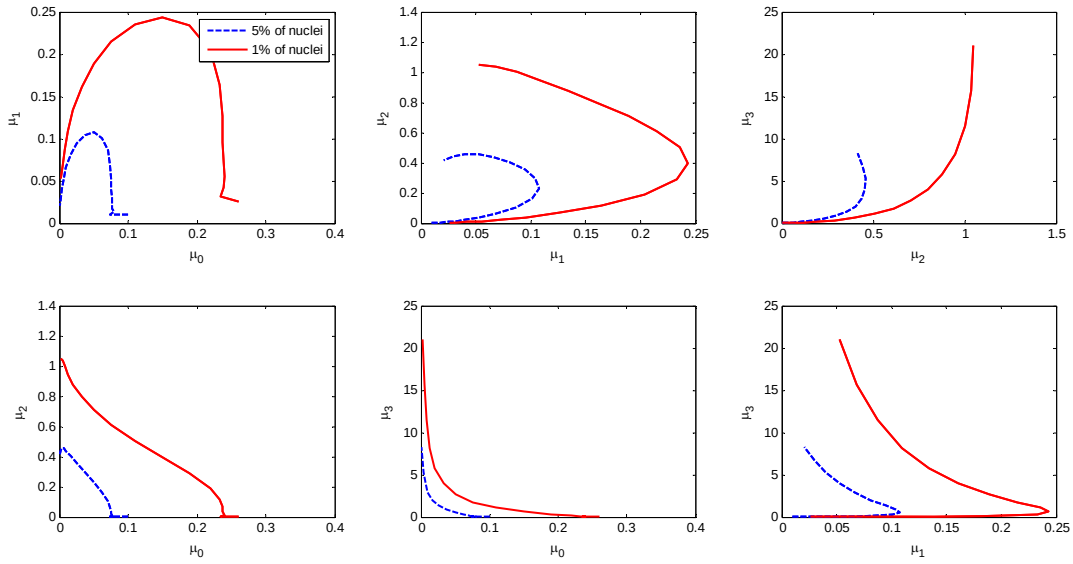

Figure 6-6 Moments contour plot using linear concentration trajectory for dimensionless system γ=1.5 and j=2. Blue dash line is for 5% of nuclei, red solid line is for 1% of nuclei.

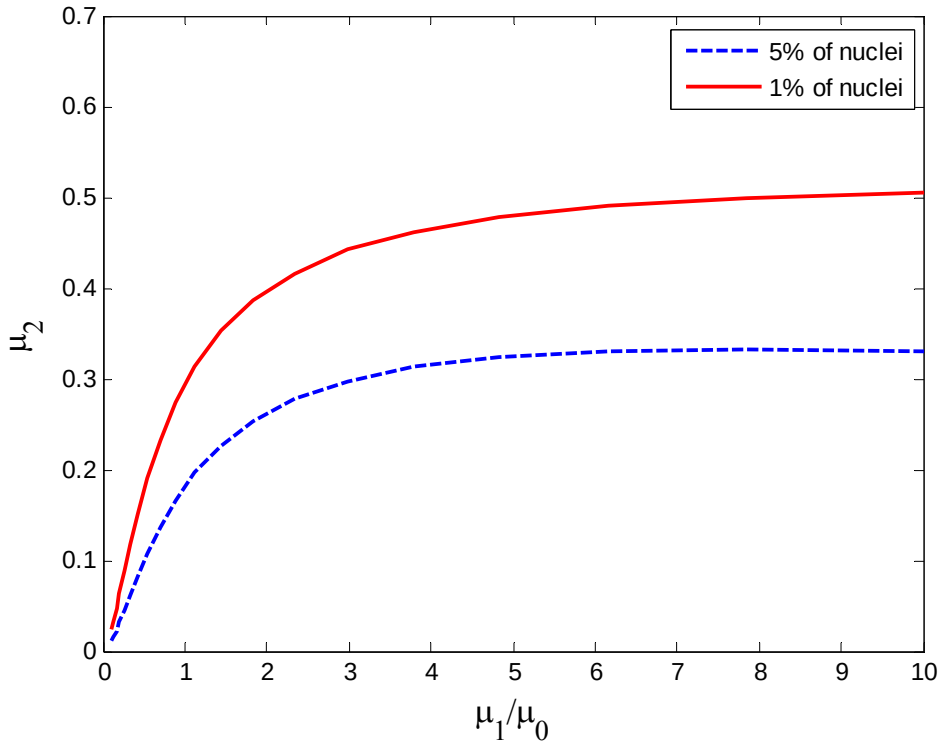

Figure 6-7 crystal total surface area versus seed number mean size L_0 with γ=3.0 and j=1.

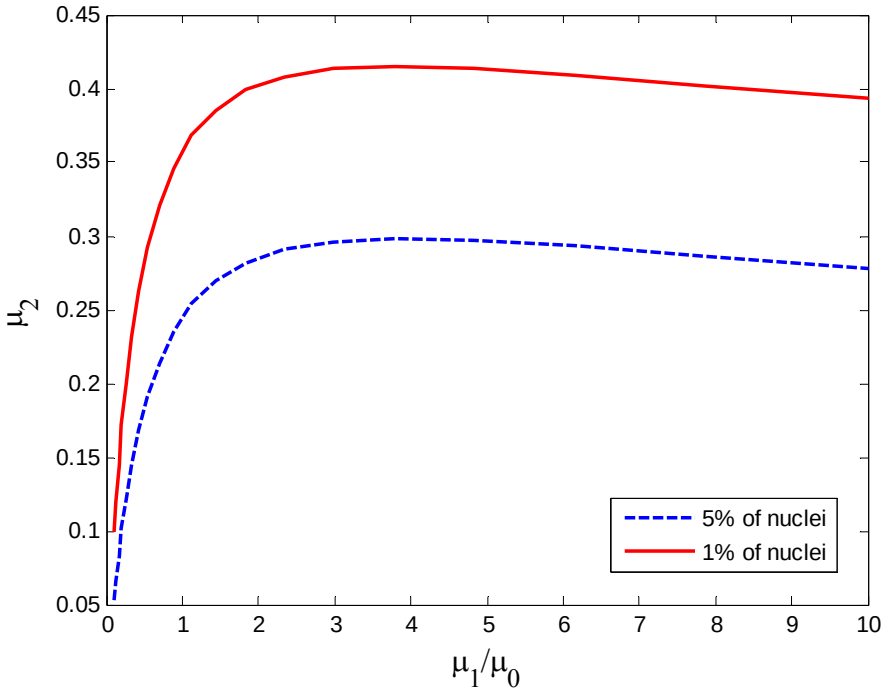

Figure 6-8 crystal total surface area versus seed number mean size L_0 with γ=3.0 and j=0.

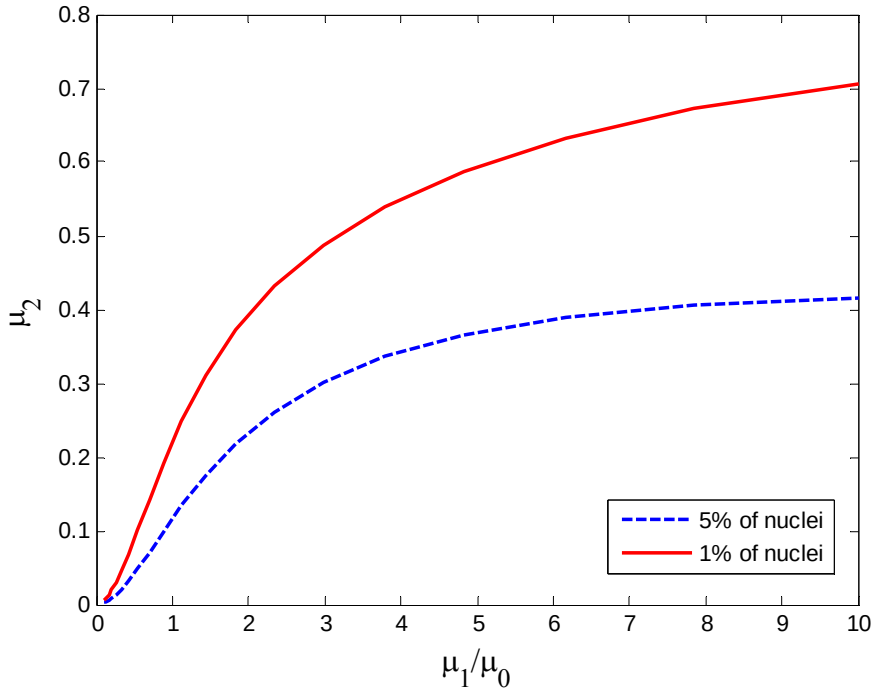

Figure 6-9 crystal total surface area versus seed number mean size L_0 with γ=3.0 and j=2.

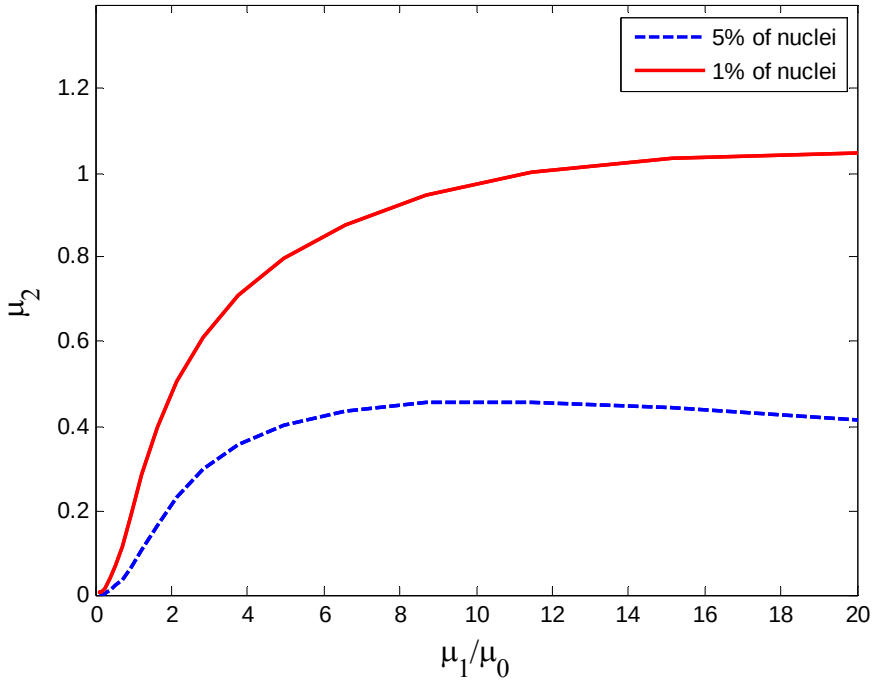

Figure 6-10 crystal total surface area versus seed number mean size L_0 with γ=1.5 and j=2.

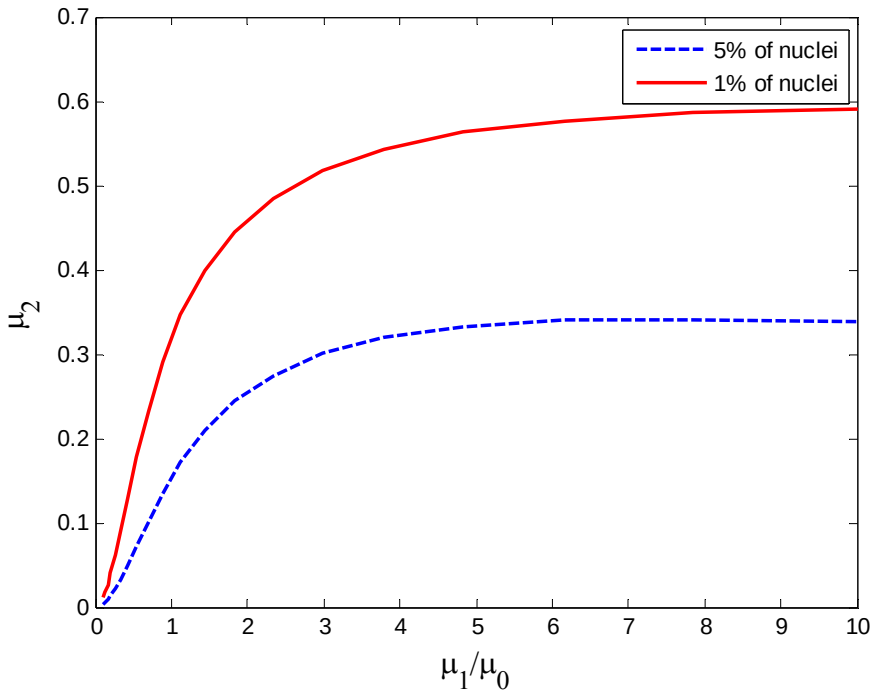

Figure 6-11 crystal total surface area versus seed number mean size L_0 with γ=1.5 and j=1.

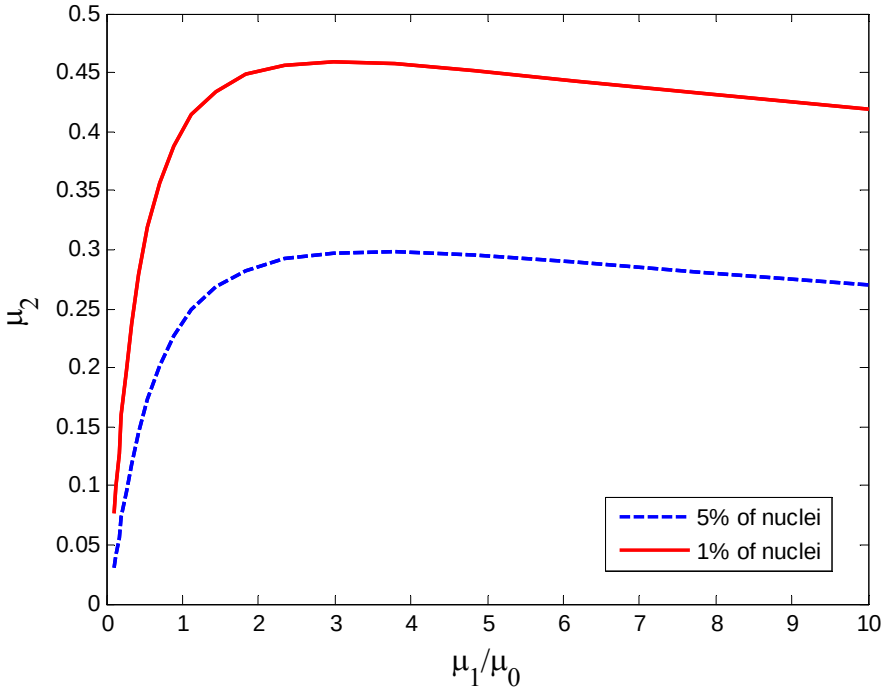

Figure 6-12 crystal total surface area versus seed number mean size L_0 with γ=1.5 and j=0.

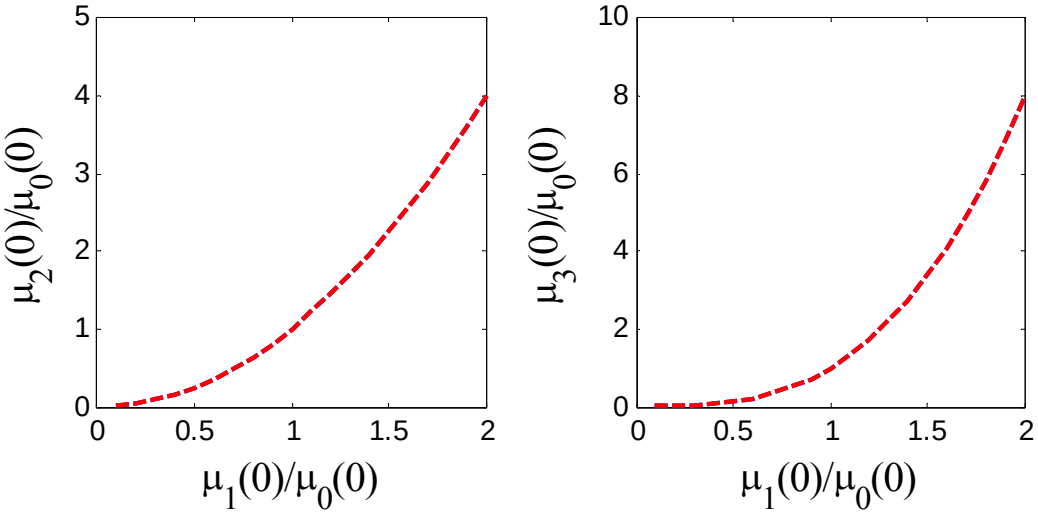

Figure 6-13 (a) Seed average surface area μ_2/μ_0 versus seed mean size μ_1/μ_0 . (b) Seed average mass μ_3/μ_0 versus seed mean size μ_1/μ_0 .

Table 6-1 Summary of critical value of μ_i from the moments contour plots of different γ and j.

Kinetic parameters		Critical value of $\mu_{i,c}$	
γ	j	$\mu_{1,c}$	$\mu_{2,c}$
3.0	1	0.35	0.52
3.0	0	>1.00	0.42
3.0	2	0.22	0.70
1.5	1	0.33	0.60
1.5	0	0.78	0.43
1.5	2	0.24	1.10

7 Relationship between batch time, seed loading, and net crystal yield

7.1 Effect of batch time t_f

This section discusses the effect of two process variables in batch crystallization: total batch time and difference between initial solution concentration and final solution concentration. In this section the target is to get a better understanding on how total batch time affects the process. First we show the effect of varying total batch time with different seed properties and use linear cooling of temperature as our temperature trajectory. In Figure 7-1 the y-axis are normalized moments, which are defined as:

$$\hat{\mu}_{i,j}(t') = \frac{\mu_{i,j}(t')}{\mu_{i,s}(0)} \tag{7-1}$$

Where i is the index of the moment and j stands for nuclei n or seed s. And x-axis is the normalized batch time, defined as:

$$t' = \frac{t}{t_f} \tag{7-2}$$

Through the definitions above, the moments for seed crystal equal to one at the beginning of process:

$$\hat{\mu}_{i,s}(t'=0)=\frac{\mu_{i,s}(0)}{\mu_{i,s}(0)}=1 \tag{7-3}$$

And for nuclei:

$$\hat{\mu}_{i,n}(t'=0)=\frac{\mu_{i,n}(0)}{\mu_{i,s}(0)}=0 \tag{7-4}$$

With these definitions we plot Figure 7-1 for seed mass is 50 kg and seed size is 100μm and seed crystal size distribution is parabolic with width equals to 20μm. About total batch time, we set to 4000s (red line), 7000s (green line) and 10000s (blue line).

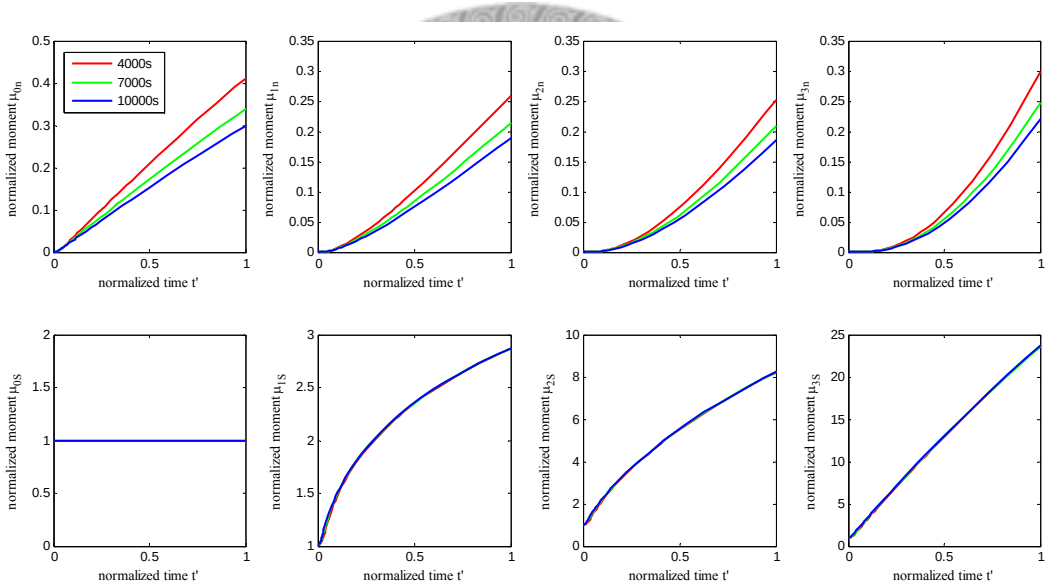

Figure 7-1 The moments plots using linear cooling temperature.

As shown in Figure 7-1 the profiles of the moments for the seed crystals (which are the figure in the second row) are similar, but as total batch time is increasing, the moments of nuclei crystal are significantly different (first row Figures). The moments indicate that the performance for large batch time is better (less nucleation) and the

reason may be the decrease of supersaturation peak as shown in Figure 7-2. Note that for three different total batch time the moments of seed crystals are almost the same.

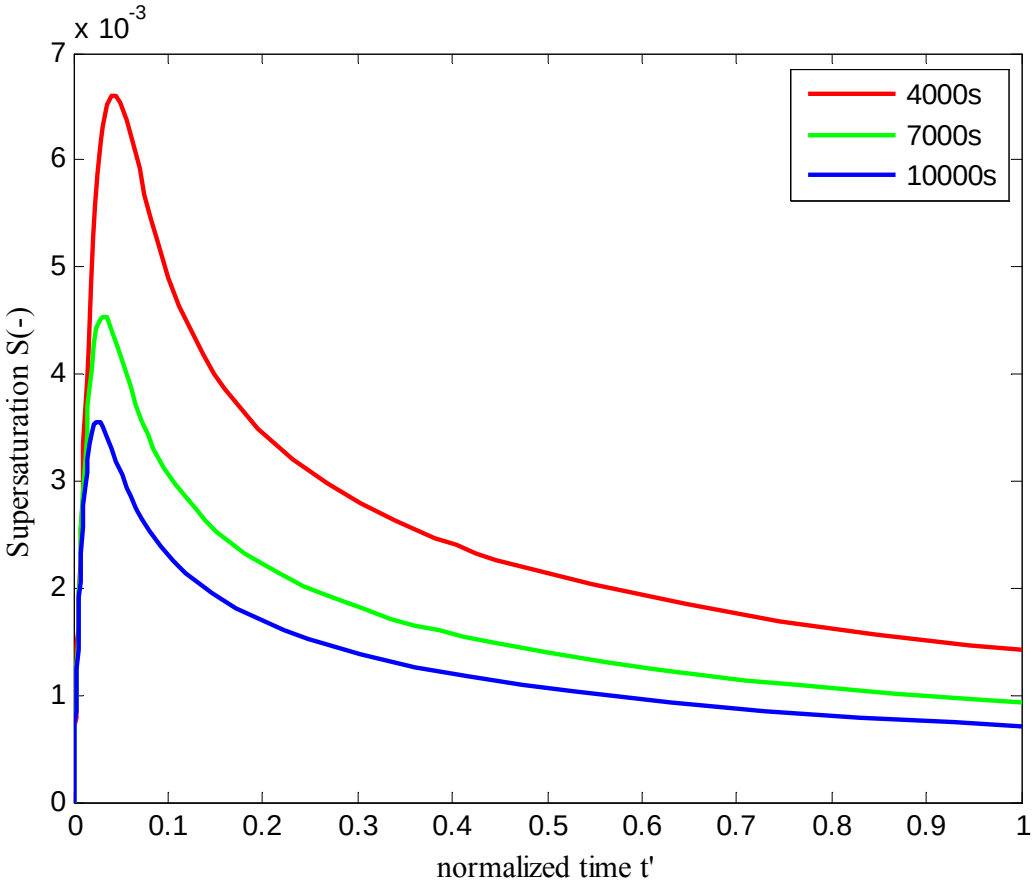

Figure 7-2 Supersaturation versus time using temperature trajectory

Next we consider another temperature trajectory called controlled cooling policy as the following definition. Note that the time dependency is cubic.

$$T(t) = T(0) + (T(t_f) - T(0))\left(\frac{t}{t_f}\right)^3 \qquad (7\text{-}5)$$

Figure 7-3 and Figure 7-4 show the results of using controlled cooling policy for the same seed properties as in Figures 7-1 and 7-2. Note that in Figure 7-4 the

maximum value of supersaturation is about 0.0035, which is smaller than linear cooling case (0.0065). And compared with the performance (here use $\mu_{3,n}$ as the standard) shown in Figure 7-1 and 7-3, controlled cooling policy is better ($\mu_{3,n} \leq 0.25$)

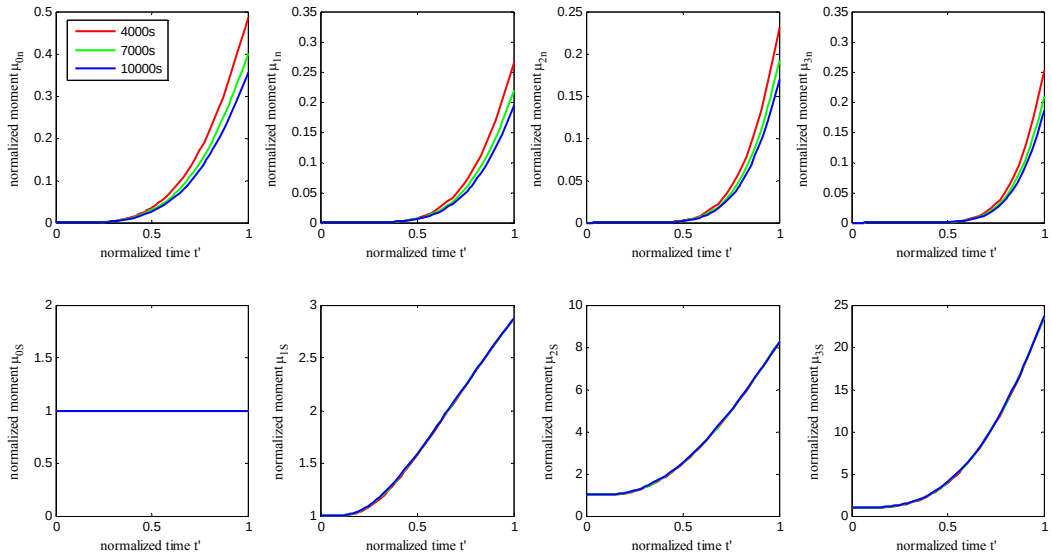

than linear cooling ($\mu_{3,n} \leq 0.30$). For both trajectories, the influence of total batch time is somehow relatively larger on nuclei crystals than on seed crystals since the

Figure 7-3 The moments plots using controlled cooling.

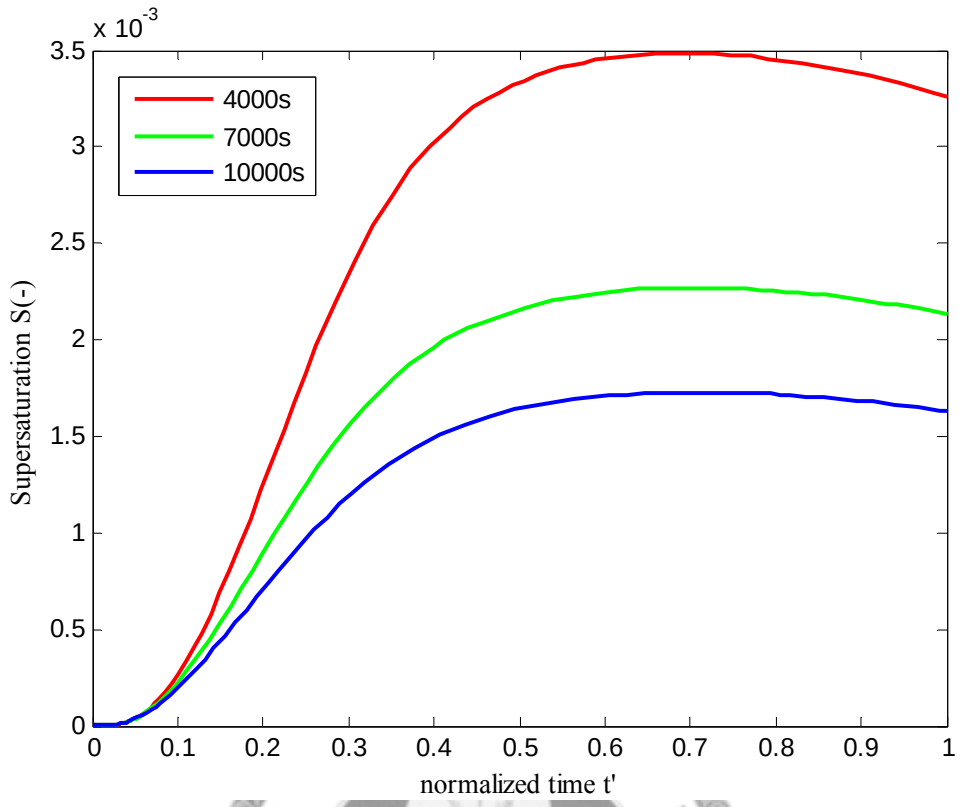

Figure 7-4 Supersaturation versus time using temperature trajectory.

nucleation rate is small so the effect on nucleation is more noticeable.

We would like to understand how total batch time t_f and seed mean size L_0 influence the critical seed loading ratio C_s^*. Figure 7-5 gives the simulation result for relationship between critical seed loading ratio C_s^* and total batch time t_f using KNO_3 system. There is significant difference in C_s^* for different batch time when seed number mean size L_0 is larger. As total batch time increases, the slopes for all three lines in Figure are smaller, giving the conclusion that C_s^* is insensitive to total batch time when total batch time is larger than 7000 sec.

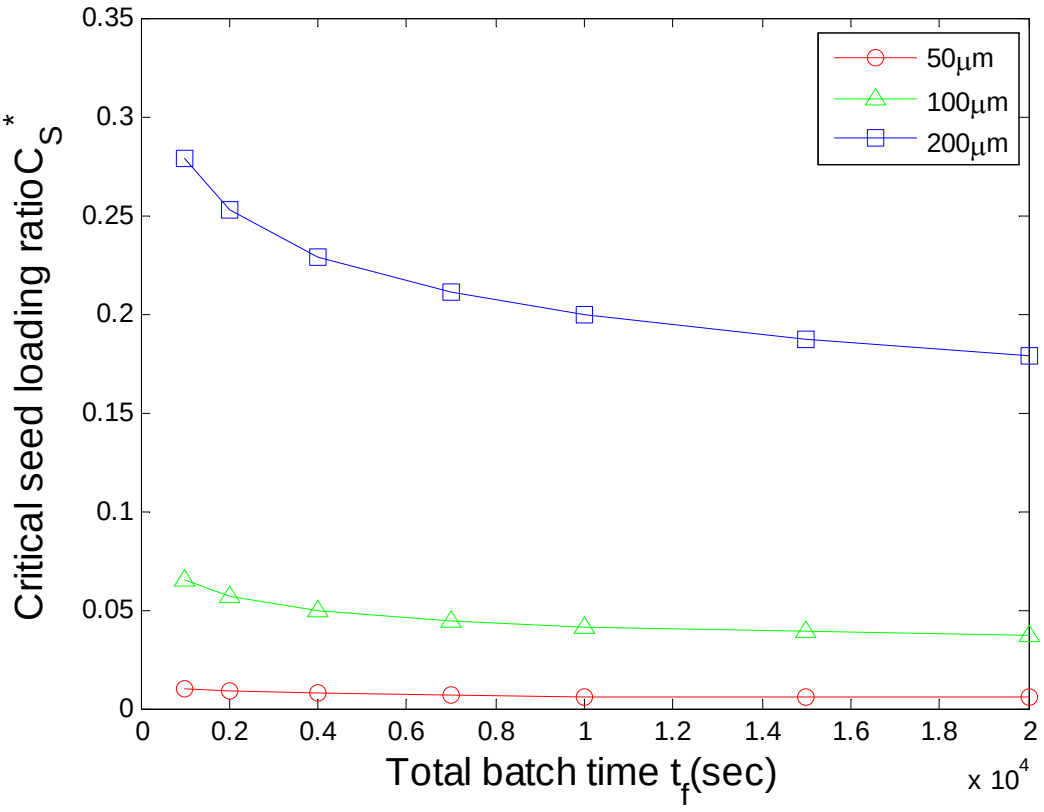

Figure 7-5 Critical seed loading ratio versus total batch time with different seed mean size.

In section 3.3 an empirical equation for C_s^* as a function of L_s was given, however it does not give information about how total batch time t_f influences C_s^*. Here we want to quantitatively determine the relationship between seed number mean size and total batch time. Recall from dimensionless variables defined by Ward et al., for dimensionless seed number mean size x_0',

$$x_0' = \frac{x_0}{\left(\bar{G}t_f\right)} \tag{7-6}$$

And the definition of reference variable for growth rate,

$$\overline{G} = \left(k_b t_f^4\right)^{\frac{-1}{\gamma+3}} \tag{7-7}$$

Where t_f is total batch time and x_0 is seed mean size, γ is ratio of b and g. We vary total batch time to see the effect of changing batch time. If the total batch time is adjusted by a factor α, i.e.

$$\hat{t}_f = \alpha t_f \tag{7-8}$$

Where $\hat{t}_f$ is new value of t_f. We desire to find the value of another parameter δ defined by

$$\hat{x}_0 = \delta \times x_0 \tag{7-9}$$

Such that if the batch time is changed to $\hat{t}_f$, then the average seed size must be changed to $\hat{x}_0$ to maintain the same critical seed loading. Substitution of the above relationship into x_0' gives,

$$x_0' = \frac{x_0}{\left(\overline{G}\hat{t}_f\right)} = \frac{x_0}{\alpha^{\left(\frac{-4}{\gamma+3}+1\right)}\left(\overline{G}\hat{t}_f\right)} = \frac{x_0}{\alpha^{\left(\frac{-4}{\gamma+3}+1\right)}\left(\overline{G}\hat{t}_f\right)} \tag{7-10}$$

Then through some derivation,

$$\delta = \alpha^{\left(\frac{-4}{\gamma+3}+1\right)} \tag{7-11}$$

In order to keep dimensionless seed mean size x_0' the same when varying to different total batch time, we have to change original seed mean size x_0 to a corresponding value by multiplying the parameter δ in Equation 7-10. Here we define

the new x_0 as “effective seed size”.

The following Tables are the simulation results of varying total batch time using Chung’s kinetic parameters. Here we do three groups of simulation tests. For three group tests seed number mean size are set to 10, 50 and 200μm respectively and α set to 1.2 and 5, then adjusting to the corresponding value of effective seed size determined by Equation 7-9 as mentioned previously. And the trajectories used are linear cooling of temperature and controlled cooling policy as mentioned before.

Table 7-1 Effect of varying total batch time t_f. Temperature trajectory is linear cooling.

α(-)	Batch Time t_f (sec)	δ(-)	Seed size x_0 (μm)	Critical seed loading(-)
1.0	1000	1.0	10	9.112×10^{-5}
1.2	1200	1.015	10.15	9.072×10^{-5}
5.0	5000	1.121	11.21	9.099×10^{-5}
1.0	1000	1.0	50	0.01033
1.2	1200	1.015	50.74	0.01030
5.0	5000	1.121	56.06	0.01041
1.0	1000	1.0	200	0.2789
1.2	1200	1.015	202.94	0.2803
5.0	5000	1.121	224.23	0.2816

Table 7-2 Effect of varying total batch time t_f. Temperature trajectory is controlled cooling.

α(-)	Batch Time t_f (sec)	δ(-)	Seed size x_0 (μm)	Critical seed loading(-)
1.0	1000	1.0	10	8.117×10^{-5}
1.2	1200	1.015	10.15	8.146×10^{-5}
5.0	5000	1.121	11.21	7.880×10^{-5}
1.0	1000	1.0	50	0.00936
1.2	1200	1.015	50.74	0.00934
5.0	5000	1.121	56.06	0.00923
1.0	1000	1.0	200	0.2633
1.2	1200	1.015	202.94	0.2654
5.0	5000	1.121	224.23	0.2653

From Tables 7-1 and 7-2, for both two trajectories the critical seed loading are almost the same (relative error is less than 1%) if the seed size is adjusted as our analysis suggested, and this result confirms our derivation. That verifies our derivation and it can be used with different temperature trajectories. However, it's also seen from the Table that the effect of total batch time on the batch crystallization is

relatively small. Note that there would be significant amount of solute left in the solution if the batch time is too short so that there is a high supersaturation value at the end of the batch. The three lines in Figure 7-6 are the results of three case studies (5kg, 25kg and 125kg of seed mass and seed number mean size are 100μm). Figure 7-6 shows that when the total batch time is smaller than about 7000 sec, concentration in the end of process is still high compared with total batch time larger than 7000 sec. The blue dash line in Figure 7-6 is the theoretical concentration in the end of process (C_f) if the supersaturation is zero.

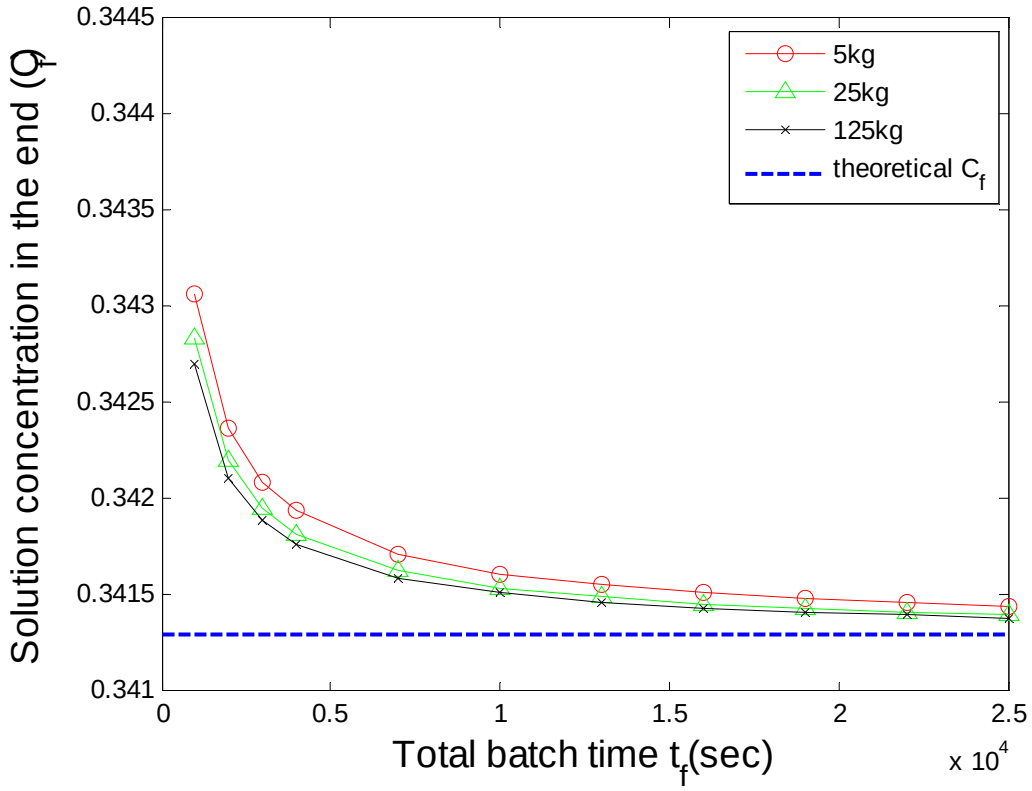

Figure 7-6 Solution concentration in the end of process

7.2 Effect of net crystal yield

This section discuss the influence of solution concentration difference C_0-C_f (which we call it solute load) on the batch process. Again recall from dimensionless variables of seed mass and the third moment,

$$m_s' = \frac{m_s}{\left(C_0 - C_f\right)} \tag{7-12}$$

$$\bar{\mu}_3 = \frac{\left(C_0 - C_f\right)}{\left(\rho_c k_v\right)} \tag{7-13}$$

From definition, if C_0-C_f is changing, $\bar{\mu}_3$ is also changed. However we cannot change only one moment and fix all other moments, because it violates the physical meaning of the moments. The definition of x_0' is independent of C_0-C_f, so changing concentration difference will not affect dimensionless seed size. But in order to keep critical seed loading the same, the seed mass should be increased to a corresponding value. Table 7-3 shows the simulation result. We do three tests of varying concentration difference by varying the difference between initial and final temperature. As concentration difference is changing, the critical seed loading ratio does not have significant change, but critical seed mass is changed to keep the critical seed loading ratio the same. Note that product size is not affected by the solute load. Another issue is that we also set batch time large enough (here is 20000 sec) to avoid

the phenomena that there is large value of supersaturation in the end of process, i.e., the production rate is much lower than our specification. From Table it also shows that the scale-up (by varying theoretical crystal yield W_{th}) of a batch crystallization process is just proportional to seed mass charged in crystallizer and we can get almost the same performance. However, scale-up may also lead to difficulty of operating the batch crystallizer.

Table 7-3 Seed size = 50 (μm) & Batch time=20000 (sec) for Chung's System.

T_0-T_f	Theoretical crystal yield (kg)	Critical seed mass (kg)	Critical seed loading(-)	Product size (μm)
5	607.11	3.1385	0.00517	244.20
15	1625.3	8.8064	0.00542	243.18
25	2383.0	12.9911	0.00545	242.89

7.3 Design guideline

From sections 7.1 and 7.2 we combine all the information and give a simple suggestion for designing batch crystallization processes and adjusting solute load C_0-C_f. If we want to increase the net crystal yield (C_0-C_f), then from the above conclusion the critical seed loading C_s* is the same. But if we want to keep the seed mass the same, then we will have a get a new C_s*, and finally from the correlation for C_s* as a function of L_s we get the seed size L_s. If we want to change the batch time but keep seed size the same, then we should find new C_s* by the Figure of C_s* vs. L_s again, then we can determine the seed mass.

8 Conclusions

In this work, we produce seed chart successfully for two different crystal systems by computer simulation, and also produce seed chart in the dimensionless system. We also analyze the effect of process variables, for example the kinetic parameter γ. When γ is large, the critical seed loading ratio is larger for a bad trajectory such as linear concentration. Another issue is the effect of varying total batch time and concentration difference between process beginning and process end. Through some derivation in dimensionless system and simulation in real crystal system (here is Chung's kinetic parameter), we confirmed our thought. Total batch time has less effect on changing into corresponding seed mean size, while changing concentration difference does not affect critical seed loading ratio C_s^* and product size. This result can be used to design a simple guideline for seeded batch crystallization process.

When a growth rate constraint is considered (chapter 3) for the dimensionless system for a particular case, results of product volume mean size VSD and crystal size distribution CSD seem to be very similar with another without the constraint. In the chapter 5 we determine empirical Equation of C_s^* versus x_0'. by simulation, and in chapter 6 we derive an analytical Equation for determining C_s^* versus x_0' with j=0 and j=1 and for all γ cases. The simulation result shows that our derivation and assumption

has high accuracy for predicting C_s^* versus x_0' of constant G trajectory. In the future we will verify with real crystal systems and these results may also work well for dimensional crystal systems.

In chapter 7, a critical seed surface area S_c, and critical value of the first moment of crystal is also observed, but generally these two variables are not recommended to be used as the design variables since the low efficiency as discussed in chapter 7. However, we can get a preliminary idea about the critical value of μ_1 and μ_2 for different kinetic exponent γ and j.

9 References

1. Jagadesh D, Kubota N, Yokota M, Sato A, Tavare NS. Large and mono-sized product crystals from natural cooling mode batch crystallizer. Journal of Chemical Engineering of Japan 1996;29(5): 865-73.
2. Jagadesh D, Chivate MR, Tavare NS. Batch Crystallization of Potassium-Chloride by an Ammoniation Process. Industrial & Engineering Chemistry Research 1992;31(2): 561-68.
3. Kubota N, Doki N, Yokota M, Sato A. Seeding policy in batch cooling crystallization. Powder Technology 2001;121(1): 31-38.
4. Doki N, Kubota N, Sato A, Yokota M, Hamada O, Masumi F. Scaleup experiments on seeded batch cooling crystallization of potassium alum. Aiche Journal 1999;45(12): 2527-33.
5. Doki N, Kubota N, Sato A, Yokota M. Effect of cooling mode on product crystal size in seeded batch crystallization of potassium alum. Chemical Engineering Journal 2001;81(1-3): 313-16.
6. Doki N, Kubota N, Yokota M, Chianese A. Determination of critical seed loading ratio for the production of crystals of uni-modal size distribution in batch cooling crystallization of potassium alum. Journal of Chemical Engineering of Japan

2002;35(7): 670-76.

7. Doki N, Kubota N, Yokota M, Kimura S, Sasaki S. Production of sodium chloride crystals of uni-modal size distribution by batch dilution crystallization. Journal of Chemical Engineering of Japan 2002;35(11): 1099-104.
8. Doki N, Yokota M, Nakamura H, Sasaki S, Kubota N. Seeded batch cooling crystallization of adipic acid from ethanol solution. Journal of Chemical Engineering of Japan 2003;36(8): 1001-04.
9. Doki N, Yokota M, Sasaki S, Kubota N. Size distribution of needle-shape crystals of monosodium L-glutamate obtained by seeded batch cooling crystallization. Journal of Chemical Engineering of Japan 2004;37(3): 436-42.
10. Kubota N, Doki N, Yokota M, Sato A. Seeding policy in batch cooling crystallization. Powder Technology 2001;121(1): 31-38.
11. Lung-Somarriba BLM, Moscosa-Santillan M, Porte C, Delacroix A. Effect of seeded surface area on crystal size distribution in glycine batch cooling crystallization: a seeding methodology. Journal of Crystal Growth 2004;270(3-4): 624-32.
12. Hojjati H, Rohani S. Cooling and seeding effect on supersaturation and final crystal size distribution (CSD) of ammonium sulphate in a batch crystallizer.

Chemical Engineering and Processing 2005;44(9): 949-57.

13. Chung SH, Ma DL, Braatz RD. Optimal seeding in batch crystallization. Canadian Journal of Chemical Engineering 1999;77(3): 590-96.
14. Mullin JW, Nyvlt J. Programmed Cooling of Batch Crystallizers. Chemical Engineering Science 1971;26(3): 369-377.
15. Ward JD, Yu CC, Doherty MF. A New Framework and a Simpler Method for the Development of Batch Crystallization Recipes. Aiche Journal 2011;57(3): 606-17.
16. Hulburt HM, Katz S. Some Problems in Particle Technology - a Statistical Mechanical Formulation. Chemical Engineering Science 1964;19(8): 555-74.
17. Mersmann, A. Ed. Crystallization Technology Handbook. New York: Marcel Dekker, 2001.
18. Nyvlt, J. Design of Crystallizers. Boca Raton, FL: CRC Press, 1992.
19. Ramkrishna D. Population Balances. San Diego: Academic Press,2000.
20. Randolph, AD. Larson MA. Theory of Particulate Processes. New York: Academic Press, 1988.
21. Tavare, NS. Industrial Crystallization: Process Simulation Analysis and Design. New York: Plenum Press, 1995.
22. Rohani S, Sarkar D, Jutan A. Multi-objective optimization of semibatch reactive

crystallization processes. Aiche Journal 2007;53(5): 1164-77.